

DiffEGG: Diffusion-Driven Edge Generation as a Pixel-Annotation-Free Alternative for Instance Annotation

Sanghyun Jo^{1,*} Ziseok Lee^{2,*} Wooyeol Lee³ Kyungsu Kim^{2,4,†}

shjo.april@gmail.com, ziseoklee@snu.ac.kr, wooyeol10519@snu.ac.kr, kyskim@snu.ac.kr

¹ OGQ, Seoul, Korea

² Department of Biomedical Sciences, Seoul National University, Seoul, Korea

³ Department of Computer Science and Engineering, Seoul National University, Seoul, Korea

⁴ School of Transdisciplinary Innovations and Interdisciplinary Program in Artificial Intelligence, Seoul National University, Seoul, Korea

Abstract

Achieving precise panoptic segmentation heavily relies on pixel-wise instance annotations, but obtaining such datasets is costly. Unsupervised instance segmentation (UIS) eliminates annotation requirements but struggles with adjacent instance merging and single-instance fragmentation, largely due to the limitations of DINO-based backbones, which lack strong instance separation cues. Weakly-supervised panoptic segmentation (WPS) reduces annotation costs by using sparse labels (e.g., points, boxes), yet these annotations remain expensive and introduce human bias and boundary errors, limiting performance. To address these challenges, we propose DiffEGG (**D**iffusion-Driven **E**dGe **G**eneration), a fully annotation-free method that extracts instance-aware features from pretrained diffusion models to generate precise instance edge maps. DiffEGG fundamentally differs from prior UIS and WPS approaches by leveraging pretrained diffusion models as a backbone. Unlike DINO-based UIS methods, diffusion models inherently capture fine-grained, instance-aware features, enabling more precise boundary delineation. DiffEGG further enhances edge connectivity through self-supervised fine-tuning, progressively improving instance separation. For WPS, DiffEGG completely eliminates annotation costs and human bias by operating without any form of manual supervision, addressing the key limitations of prior best methods. Additionally, we introduce RIP, a post-processing technique that fuses DiffEGG’s edge maps with segmentation masks in a task-agnostic manner. This broad applicability allows DiffEGG to be seamlessly integrated into various segmentation frameworks. When applied to UIS, DiffEGG and RIP achieve an average +4.4 AP improvement over prior best UIS methods. When combined with weakly-supervised semantic segmentation (WSS), DiffEGG enables WPS without instance annotations, outperforming prior best point-supervised WPS methods by +1.7 PQ. These results demonstrate that DiffEGG’s edge maps serve as a cost-effective, annotation-free alternative to instance annotations, significantly improving segmentation without human intervention. Code is available at <https://github.com/shjo-april/DiffEGG>.

1 Introduction

Panoptic segmentation—unifying semantic and instance segmentation—is crucial for numerous applications, such as autonomous driving [10, 77, 13]. However, achieving high-quality segmentation typically requires dense pixel-level annotations, making large-scale dataset creation costly and labor intensive.

Among different annotation types, instance annotations are the most expensive because of the need for precise instance-wise labeling. The minimal form of annotation is class-level image tags, which only indicate the presence of objects without specifying their locations or counts. While weakly supervised semantic segmentation (WSS) with image tags demonstrate near-parity with fully supervised models, achieving 99% of their performance [28], weakly supervised panoptic segmentation (WPS) with image tags lags at 52% of fully supervised results [62, 9], highlighting the need for stronger supervision.

Recent methods using additional point annotations improve performance (up to 73% of fully supervised results) [40, 9], but they suffer from the following:

*Equal Contribution

†Corresponding Author

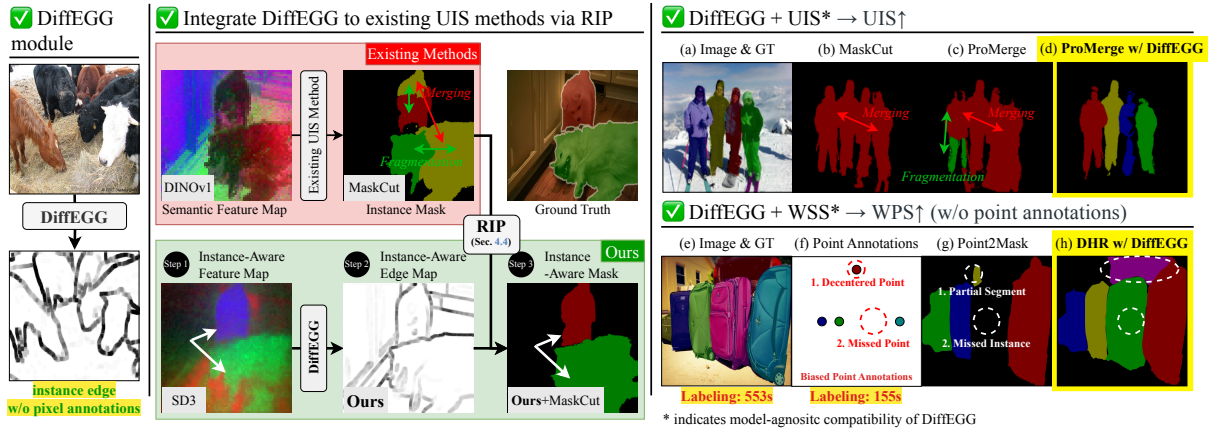


Figure 1: **Overview of DiffEGG and its broad applicability.** (*Left*) DiffEGG extracts fine-grained, instance-aware edge maps from pretrained diffusion models, enabling precise boundary delineation. (*Middle*) We introduce a post-processing technique, RIP, to fuse DiffEGG generated edge maps with existing segmentation masks for improved instance separation in unsupervised instance segmentation (UIS) tasks. (*Right-Top*) By combining DiffEGG with UIS, we improve instance masks in model-agnostic manner; (a) GT, (b) MaskCut [67] with adjacent instance merging, (c) ProMerge [36] with both adjacent instance merging and single instance fragmentation, (d) DiffEGG with UIS method (e.g., ProMerge [36]) effectively separates instances, addressing merging and fragmentation. (*Right-Bottom*) By combining DiffEGG with weakly-supervised semantic segmentation (WSS), we achieve weakly-supervised panoptic segmentation (WPS) only with image tags; (e) GT, (f) inconsistent point annotations showing partial/missed instances, (g) Point2Mask [40] with annotation-induced failures, (h) DiffEGG with WSS method (e.g., DHR [28]) outperforms point-supervised methods [40] while requiring solely image tags.

1. **Insufficient boundary information:** Point annotations are placed at object centers, providing no explicit instance boundaries. This leads to a failure to separate adjacent instances, causing segmentation merge errors.
2. **Human bias:** Point placements are subjective, leading to annotation-induced errors. Missed points result in missing instance masks, while inaccurately placed points lead to fragmented instances. Such biases are particularly problematic in datasets with multiple instances per image (e.g., COCO [45]).

Unsupervised instance segmentation (UIS) offers an alternative to point annotations by leveraging feature representations from pretrained vision transformers (e.g., DINO), but it faces two challenges (Fig. G):

1. **Problem A. Adjacent instance merging:** DINO-based methods primarily capture semantic features, making it difficult to distinguish instances of similar categories (e.g., multiple dogs).
2. **Problem B. Single instance fragmentation:** UIS methods rely on hyperparameters that determine the number of instances and the granularity of partitioning, leading to inconsistent segmentation quality.

To consistently enhance both UIS and WPS methods, we propose **DiffEGG**—a **Diff**usion-driven **EdG**e **Ge**neration framework—that leverages pretrained diffusion models to generate instance-aware edge maps without manual annotations. Our approach is motivated by two key observations about text-to-image diffusion models [14, 55]:

- **Observation 1:** Text-to-image diffusion models [55] can generate a specified number of instances based on prompts (e.g., “a cat” vs. “two cats”).
- **Observation 2:** Their early stage self-attention maps reveal distinct instance-level structures, evolving through a structured progression (see Fig. 2):

Noise \rightarrow Instance Information \rightarrow Semantic Information

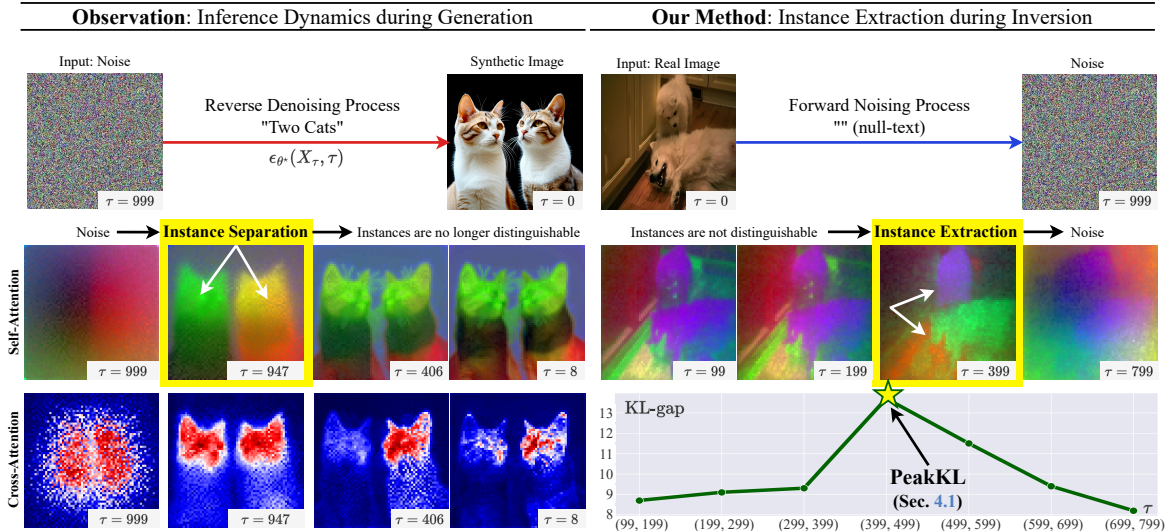


Figure 2: **Inference dynamics in text-to-image diffusion models.** (*Left*) We observed that self-attention maps obtained from earlier timesteps during the reverse process exhibit information that can be used to separate adjacent instances. (*Right*) We apply our observation to extract instance information from self-attention maps during the forward noising process. Since DiffEGG does not utilize any text supervision, the noising process is carried out with null-text, taking away the utility of cross-attention maps. (*Bottom Right*) Finally, we propose a novel stopping rule, PeakKL that automatically stops at the optimal timestep when adjacent instances are fully distinguishable. The graph plots the KL-gap between consecutive self-attention maps. The peak at (399, 499) means the KL-gap between 499 and 399 is the greatest, hence 399 is our desired timestep. Note that all PCA visualizations of diffusion features are obtained from SD3 [14].

Building on these insights, DiffEGG employs a parameter-free stopping rule (PeakKL, Section 4.1) to pinpoint the optimal diffusion timestep for clear instance boundaries, then applies a novel scoring method (EdgeKL, Section 4.2) to convert these maps into precise edge maps. A fine-tuning procedure (Section 4.3) further enhances edge connectivity and a propagation technique, RIP (Section 4.4), integrates these edges with segmentation masks from existing UIS and WSS methods [67, 27, 28].

DiffEGG’s edge-focused, annotation-free approach enables precise boundary generation between adjacent instances, effectively overcoming *adjacent instance merging*. Using the edge map, DiffEGG determines fragmented masks that belong to the same instance and merges them, resolving *single instance fragmentation* —all without any human annotations. Overcoming such limitations of UIS enables DiffEGG+WSS, which only uses image tags, to outperform panoptic segmentation methods [40, 16] that require point annotations in addition to tags. Remarkably, despite relying on less supervision, DiffEGG+WSS achieves superior panoptic segmentation quality, demonstrating that precise edge generation can compensate for the lack of instance annotations in panoptic segmentation.

Our key contributions are:

- We propose **DiffEGG** a novel two-stage framework which generates instance-aware edge maps using a pretrained diffusion model.
 1. **Pixel-Annotation Free Instance Edge Generation.** We propose PeakKL, a temporal metric, and EdgeKL, a spatial metric, which together enable the automatic generation of initial edge maps from instance-aware feature maps of the diffusion model, detecting boundaries between adjacent instances.
 2. **Self-Supervised Fine-tuning for Edge Connectivity.** We introduce a diffusion fine-tuning strategy to improve edge connectivity recursively, achieving adjacent instance discrimination and resolving mask fragmentation issues with our refined edge map.
- **Model-Agnostic UIS Enhancement by DiffEGG.** Extensive experiments demonstrate that DiffEGG’s edge maps significantly improve the performance of existing UIS methods by +4.4 AP on average, with negligible (< 6%) computational overhead during inference (see Table 1 and Table F).
- **Panoptic Segmentation with Tags.** DiffEGG+WSS shows strong results in weakly-supervised

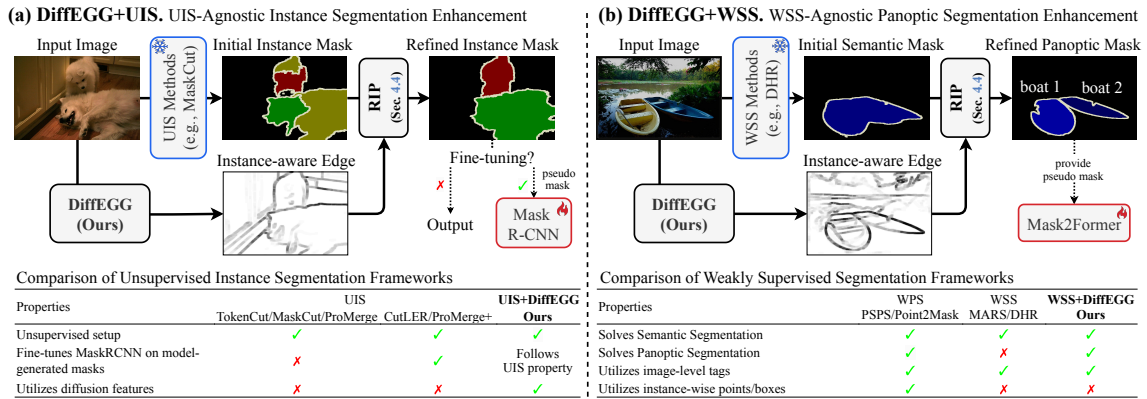


Figure 3: DiffEGG (Ours) integrated into existing Unsupervised Instance Segmentation (UIS) and Weakly Supervised Panoptic Segmentation (WPS) pipelines. The input image is initially segmented via an existing UIS or WSS method. By integrating DiffEGG-generated edge maps via random walk-based instance propagation (RIP), we enhance (a) UIS and (b) WPS performance in a model-agnostic manner.

panoptic segmentation, outperforming point-supervised methods with just tags and zero additional inference time (see Table 2).

2 Related Work

This section reviews recent developments in unsupervised instance segmentation, weakly supervised panoptic/semantic segmentation, and diffusion models applied to segmentation, highlighting how DiffEGG differs from existing approaches from both literatures. We describe a comprehensive review of recent studies in Appendix B.

2.1 Unsupervised Instance Segmentation

Instance segmentation (IS) aims to delineate individual objects in images, typically relying on labor-intensive pixel-level annotations [9]. To improve scalability, recent studies [5, 51, 68] have explored unsupervised and text-supervised methods (e.g., using CLIP [56]). Specifically, SOLO-based approaches [66, 24] rely on CNN-based (e.g., DenseCL [65]) pseudo-mask generation but show poor performance and require training from scratch, making them computationally expensive. MaskCut [67] and ProMerge [36] apply feature clustering with the graph cut algorithm [69] on pretrained self-supervised vision transformers (e.g., DINOv1 [5]) to separate instances. In contrast, DiffEGG adopts an edge-oriented strategy that leverages generative text-to-image diffusion models [53, 3, 14, 55] to directly extract instance boundaries from early denoising stages.

2.2 Weakly Supervised Segmentation

Panoptic segmentation (PS) unifies semantic and instance segmentation, but fully supervised methods [42, 78, 8, 41, 32, 73] including Mask2Former [9] require dense pixel-wise annotations.

Weakly supervised semantic segmentation (WSS) [29, 27, 58, 31, 35, 12, 75, 82, 46, 60, 26, 74, 37, 48, 7, 72] uses minimal supervision (image-level tags) to generate class activation maps (CAMs) that highlight object regions. Despite achieving near-parity with fully supervised models in semantic segmentation, WSS lacks instance-level information, making it insufficient for panoptic segmentation. Weakly supervised panoptic segmentation (WPS) [40, 16, 38, 39, 25] incorporate additional instance-level annotations such as points or bounding boxes to generate pseudo-panoptic masks, which replace human-annotated masks for training panoptic models [9]. However, the reliance on manually annotated points and boxes remains expensive and error-prone.

DiffEGG circumvents these issues by extracting instance-aware edge maps without additional manual cues, enhancing WSS pipelines to deliver tag-supervised WPS that outperforms methods reliant on additional (point or box) annotations. Our work bridges the gap between WSS and WPS by offering an annotation-free instance-aware refinement mechanism. By leveraging diffusion models’ rich feature representations, DiffEGG achieves superior segmentation quality without additional human supervision, setting a new paradigm for weakly supervised panoptic segmentation.

2.3 Diffusion Models Applied to Segmentation

Recent works such as DiffCut [11] and DiffSeg [64] exploit self-attention maps from text-to-image diffusion models [53, 3, 14, 55] for semantic segmentation. While DiffCut [11] uses Normalized Cuts on diffusion embeddings with sensitive threshold tuning to generate pixel groups, and DiffSeg extracts semantic regions from self-attention layers with limited instance detail, these methods target semantic rather than instance segmentation. DiffEGG uniquely harnesses early-stage diffusion features to produce instance-aware edge maps, bridging the gap between semantic and instance segmentation.

2.4 Open Vocabulary Segmentation

Recent methods combining multimodal models (MLLM/VLM) with segmentation frameworks, such as SAM [33], have enabled open-vocabulary panoptic segmentation. Early approaches utilizing CLIP [56] demonstrated that free-form text prompts can guide segmentation [80, 6]; however, these methods generally underperform compared to specialized segmentation models that rely on precise mask annotations [9]. More recent advancements, such as Grounding DINO [49] and Ferret [76], have incorporated box annotations and language models to improve detection. Despite this progress, these models often struggle to generate accurate instance seeds from multi-tag inputs, failing to distinguish visually similar classes. In contrast, advanced weakly supervised methods, like DHR [28], have demonstrated stronger multi-class prediction performance. Our experiments show that DiffEGG, by leveraging robust weakly supervised signals, outperforms these open-vocabulary methods in segmentation accuracy (see Table 2 for details).

3 Preliminaries

This section provides a mathematical description of diffusion models, the denoising process, and self-attention maps. A majority of mathematical notations used in the rest of the paper are defined in this section.

3.1 Diffusion Models and the Denoising Process

Diffusion models use two processes to learn and generate images: a forward process that gradually applies noise to an image and a reverse denoising process that reconstructs the original image by progressively removing noise. This bidirectional framework is mathematically defined through stochastic differential equations (SDEs) [63]. Let $X_0 \sim p_0$ represent a sample from the target image domain (e.g., ImageNet [34]) and $\bar{X}_T \sim p_T$ represent the final noised image after the forward process. We assume that p_T is given as a prior. Typically, the model is chosen such that it approaches a Gaussian distribution for sufficiently large T . The equations governing the diffusion process are as follows:

1. **Forward Process:**

$$\begin{cases} dX_t = -\beta_t X_t dt + \sigma_t dW_t \\ X_0 \sim p_0 \end{cases} \quad (1)$$

where β_t and σ_t are time-dependent coefficients, and W_t is the forward-time Brownian motion.

2. **Reverse Process:**

$$\begin{cases} d\bar{X}_t = [-\beta_t \bar{X}_t - \sigma_t^2 \nabla \log p_t(\bar{X}_t)] dt + \sigma_t d\bar{W}_t \\ \bar{X}_T \sim p_T \end{cases} \quad (2)$$

where \bar{W}_t is the reverse-time Brownian motion.

In practice, the continuous forward process is discretized into T timesteps and discrete timestep coefficients $\bar{\alpha}_t$ are chosen such that:

$$X_t = \sqrt{\bar{\alpha}_t} X_0 + \sqrt{1 - \bar{\alpha}_t} \epsilon \quad (3)$$

where $\epsilon \sim \mathcal{N}(0, I)$, $t = 1, \dots, T$. A neural network, $\epsilon_\theta(X, t)$, estimates the noise ϵ for the reverse process by solving the optimization problem $\theta^* = \operatorname{argmin}_{\theta \in \Theta} \mathbb{E}_{\epsilon, t, X_0} \|\epsilon_\theta(X_t, t) - \epsilon\|_2^2$. After (3), we have a noised

image, $X_t \sim p_t$, which undergoes a reverse transformation to produce a denoised prediction \hat{X}_0 of the original image.

$$\hat{X}_0 = \frac{1}{\sqrt{\bar{\alpha}_t}} (X_t - \sqrt{1 - \bar{\alpha}_t} \epsilon_{\theta^*}(X_t, t)) \quad (4)$$

In this paper, we write $\text{Reconstruct}(\epsilon_\theta, X_0, t)$ to denote the process of sampling Gaussian noise, adding noise to X_0 via (3), and finally reconstructing the image via (4).

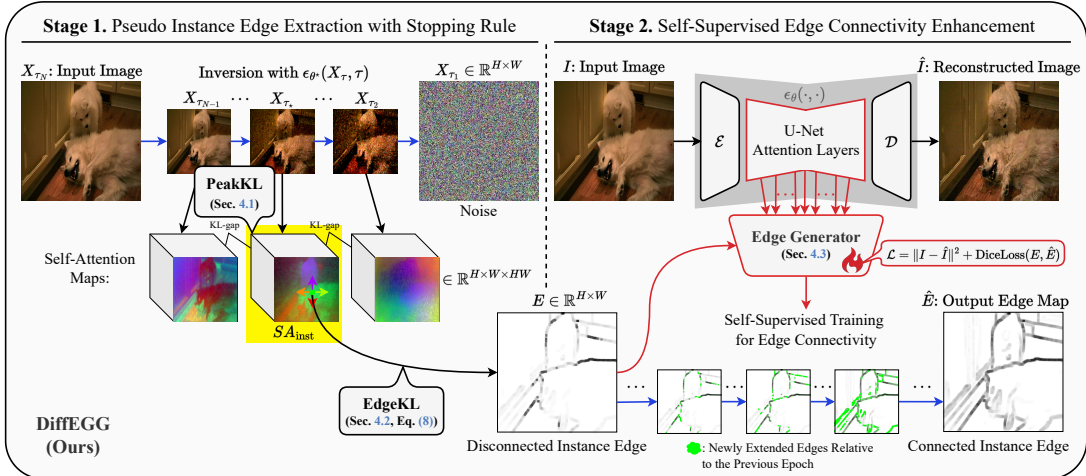


Figure 4: **Overview of DiffEGG.** Given an input image I , we apply iterative noise addition to generate self-attention maps, capturing progression in instance details. Using our stopping rule, PeakKL, we determine the optimal point where distinct instance information peaks, obtaining SA_{inst} . With EdgeKL, we produce a pseudo edge map E , which may be disconnected and incomplete. To address this, we use E as self-supervision to train an edge generator and fine-tune the diffusion model. After fine-tuning, DiffEGG returns a connected edge map \hat{E} for any given image.

3.2 Self-Attention Maps in Diffusion Models

The architecture of $\epsilon_\theta(X, t)$ in text-to-image diffusion models consists of an encoder \mathcal{E} , a decoder \mathcal{D} , and multiple transformer layers.

Encoder and Decoder Layers. A high-resolution image I and caption c are encoded into a lower-resolution latent representation. Let $X_0 = \mathcal{E}(I)$. From then on, the model applies the forward and reverse diffusion processes on X_0 and learns to predict the noise for the latent conditioned on the caption embedding. Finally, the reconstructed latent is decoded back to the image dimension via $\hat{I} = \mathcal{D}(\hat{X}_0)$. These models not only minimize reconstruction loss but also learn to generate images conditioned on captions.

Transformer Layers. Self-attention maps $SA(X)$ (see Appendix C.1) play a key role in capturing spatial dependencies within an image during the diffusion process, while cross-attention maps capture the dependencies between the caption and image. Since DiffEGG assumes an unsupervised setting, all captions are given as null-text (“”). Therefore, we focus solely on self-attention maps.

Hooker Function. A hooker function \mathcal{H} , implemented in PyTorch, enables inspection of intermediate model layers, particularly self-attention layers. Every time the layer performs a forward pass, \mathcal{H} extracts the attention map without altering the model’s behavior. We use $\mathcal{H}(\epsilon_\theta, X_0, t)$ to denote the accumulated attention map evaluated during the forward pass at timestep t given input X_0 (see Appendix C.1 for details on accumulating attention maps).

4 Method

In this section, we detail how DiffEGG extracts instance-level information directly from early self-attention maps in diffusion models and transforms them into pseudo-edge maps. We then introduce a diffusion fine-tuning strategy to enhance edge connectivity and a propagation method to obtain instance and panoptic masks (see Fig. 4).

4.1 PeakKL: DiffEGG’s Stopping Rule

During image generation, early self-attention maps are dominated by noise. As denoising progresses, a pronounced peak in the KL divergence between consecutive maps signals the emergence of structured instance-level features, where the model begins to differentiate individual instances. After this peak,

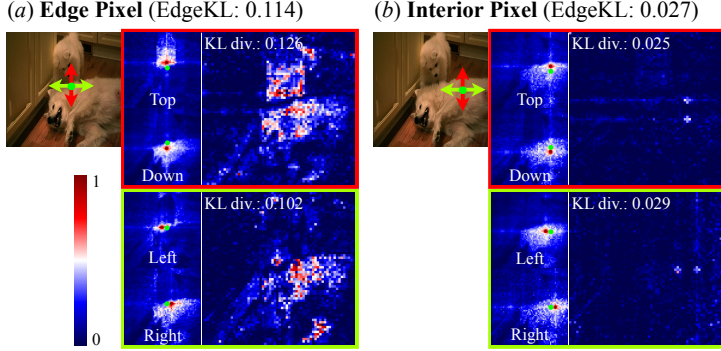


Figure 5: **Illustration of EdgeKL.** EdgeKL measures the KL gap between top & bottom, left & right self-attention features for every pixel in the image. (a) EdgeKL is large for edge pixels. (b) EdgeKL is small for interior pixels.

further denoising changes minor details without significantly altering the image structure, resulting in smaller KL gaps (see Fig. 2).

Leveraging our findings, PeakKL simply identifies the optimal timestep n^* with the largest KL divergence between consecutive self-attention maps (see Algorithm 1 in Appendix C.2):

$$n^* = \underset{n}{\operatorname{argmax}} D_{\text{KL}}(SA[n+1] \parallel SA[n]) \quad (5)$$

At n^* , $SA[n^*]$ captures clear object boundaries; we denote this instance-aware self-attention map as SA_{inst} .

4.2 EdgeKL: Scoring for Edge Confidence

Building on PeakKL, we introduce EdgeKL as a scoring method to determine edge confidence. SA maps obtained at the PeakKL timestep capture meaningful spatial relationships within instances. Specifically, pixels belonging to the same object tend to have similar feature maps, resulting in a small KL divergence. Conversely, even if adjacent, pixels belonging to different objects exhibit distinct feature maps with a more significant KL divergence.

With this insight, EdgeKL quantifies edge confidence by measuring KL divergence between self-attention features of neighboring pixels. For a pixel in position (i, j) , EdgeKL is defined as the sum of the KL divergence between the SA features of its top/down and left/right neighboring pixels:

$$\begin{aligned} \text{EdgeKL}(i, j; SA) := & D_{\text{KL}}(SA[i+1, j] \parallel SA[i-1, j]) \\ & + D_{\text{KL}}(SA[i, j+1] \parallel SA[i, j-1]) \end{aligned} \quad (6)$$

As illustrated in Fig. 5, high EdgeKL scores indicates likely instance boundaries, while lower values correspond to interior regions. Pixels are then classified based on their score relative to the mean (μ) and standard deviation (σ) of the EdgeKL score distribution: scores above $\mu + \sigma$ are marked as edges (1), below as interior (0), and in between as uncertain (-1) (see Algorithm 2 in Appendix C.2).

4.3 Self-Supervised Edge Enhancement

The initial edge map from EdgeKL can be fragmented due to uncertain pixels. To improve continuity (see Fig. 6), we apply diffusion fine-tuning using LoRA [23] along with an edge generator module [71].

Our approach fine-tunes the transformer layers of a text-to-image latent diffusion model with LoRA and trains a new edge generator \mathcal{G}_ϕ from scratch (see Appendix C.3). This self-supervised process requires no extra annotations. The training objective combines image reconstruction loss and Dice loss, $\mathcal{L} = \|I - \hat{I}\|^2 + \text{DiceLoss}(E, \hat{E})$, where

$$\text{DiceLoss}(E, \hat{E}) = 1 - \frac{2 \sum W_{i,j} E_{i,j} \hat{E}_{i,j}}{\sum W_{i,j} E_{i,j}^2 + \sum W_{i,j} \hat{E}_{i,j}^2} \quad (7)$$

and the weighting $W_{i,j}$ excludes uncertain pixels:

$$W_{i,j} = \begin{cases} 0 & \text{if } E_{i,j} = -1 \\ 1 & \text{otherwise} \end{cases} \quad (8)$$

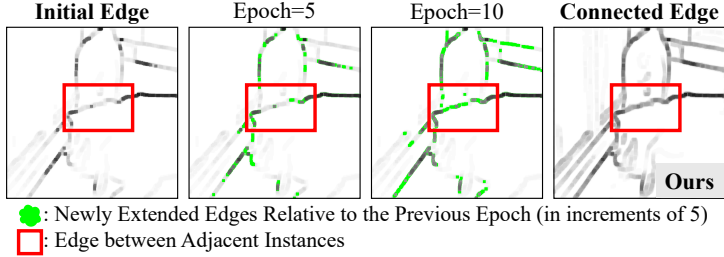


Figure 6: **Effect of fine-tuning for enhancing edge connectivity.** Initially, edges appear fragmented and incomplete. Our fine-tuning technique iteratively resolves incomplete boundary predictions, ensuring continuous edge connectivity. Green regions in the edge map indicate the added edges when comparing previous edge maps with an epoch difference of 5. The rightmost edge map, after the entire fine-tuning, displays the fully connected edges.

Here, $I, \hat{I} \in \mathbb{R}^{H \times W \times 3}$ denote the original and reconstructed images, respectively. $E \in \{0, 1, -1\}^{H \times W}$ is the pseudo-instance edge from EdgeKL and $\hat{E} \in [0, 1]^{H \times W}$ is the predicted edge map from the edge generator. We exclude uncertain pixels (where $E = -1$) from the dice loss computation via W to allow the model to focus on confident edge and interior points.

4.4 Post-Generation Processing Techniques

Once precise edges are generated, we refine instance or semantic masks from existing UIS/WSS methods using *Connected Component Labeling (CCL)* and *Random Walk-Based Instance Propagation (RIP)*. CCL [59] leverages DiffEGG-generated edges to delineate clear instance boundaries, while RIP, adapted from AffinityNet [2, 1], smooths and extends instance regions by allowing overlaps between fragments of the same instance (see Fig. 1).

To handle fragmentation, we iteratively merge masks with an IoU above 0.5 until no further merges occur, resulting in complete and accurate instance masks. Details on RIP and its usage in applying DiffEGG to segmentation are provided in Appendix C.4.

5 Experiments

We evaluate DiffEGG on unsupervised instance segmentation (UIS) and weakly supervised panoptic segmentation (WPS) using standard benchmarks. All experiments run on a single NVIDIA A100 GPU following established UIS/WPS protocols [67, 36, 40] (see Appendix E for details). For our evaluations, we primarily use the SD3.5-L [14] diffusion backbone.

5.1 Implementation Details

We integrate DiffEGG into existing UIS/WPS pipelines by combining three interchangeable components: the diffusion backbone, a base UIS method, and a base WSS method. For fair comparisons with existing UIS models fine-tuned on ImageNet [34], we also fine-tune our diffusion model and edge generator on ImageNet. This allows DiffEGG-based instance edges to be applied directly to other datasets (e.g., VOC2012 [15], COCO2014 [44]) without further fine-tuning. For WPS experiments, we employ two separately fine-tuned diffusion models for each dataset (VOC and COCO).

5.2 Application 1: Improving UIS with DiffEGG

We apply DiffEGG to enhance instance masks generated by existing UIS methods (MaskCut [67], ProMerge [36], CutLER [67] and ProMerge+ [36]) via our edge refinement pipeline (Algorithm 4). Qualitative results in Figs. O and P show that DiffEGG consistently separates adjacent instances and significantly improves overall segmentation quality. DiffEGG enhances both base and fine-tuned methods seamlessly, achieving an average gain of +4.4 AP. To clarify, DiffEGG is fine-tuned specifically for edge prediction, whereas UIS fine-tuning (e.g., in ProMerge+ [36]) relies on training MaskRCNN [22] using model-generated pseudo masks.

5.3 Application 2: DiffEGG-supervised WPS

For WPS, we refine masks generated by WSS methods, namely MARS [27] and DHR [28], via Algorithm 4 using our edge refinement method (RIP in Section 4.4). Next, we train conventional panoptic

Table 1: **Unsupervised instance segmentation (UIS) performance comparison on multiple benchmarks.** We evaluate performance improvements brought by DiffEGG when combined with base UIS methods (MaskCut, ProMerge) as well as their fine-tuned variants (CutLER, ProMerge+). DiffEGG consistently improves both base and fine-tuned approaches.

Method	VOC 2012		COCO 2014		COCO 2017		Method	VOC 2012		COCO 2014		COCO 2017		
	AP ^{mk}	AR ^{mk} ₁₀₀	AP ^{mk}	AR ^{mk} ₁₀₀	AP ^{mk}	AR ^{mk} ₁₀₀		AP ^{mk}	AR ^{mk} ₁₀₀	AP ^{mk}	AR ^{mk} ₁₀₀	AP ^{mk}	AR ^{mk} ₁₀₀	
Base UIS	MaskCut [67]	5.8*	14.0*	3.0*	6.7*	2.3*	6.5*	ProMerge [36]	5.0*	13.9*	3.1*	7.6*	2.5*	7.5*
	+ DiffEGG (Ours)	9.7	18.4	7.9	12.6	7.5	9.8	+ DiffEGG (Ours)	9.4	18.2	8.2	13.1	7.8	11.2
Fine-tuned UIS	CutLER [67]	11.2*	34.2*	8.9*	25.1*	8.7*	24.9*	ProMerge+ [36]	11.1*	33.1*	9.0*	25.3*	8.9*	25.1*
	+ DiffEGG (Ours)	14.8	45.3	13.1	34.6	12.8	33.9	+ DiffEGG (Ours)	15.0	43.8	13.3	35.1	13.0	25.8

* Reproduced results using publicly accessible code for a fair comparison. The rest are the values reported in the publication.

Table 2: **Panoptic segmentation (PS) performance comparison on multiple benchmarks.** In our PS evaluation setup, DiffEGG leverages semantic masks generated by MARS/DHR. Remarkably, DHR+DiffEGG outperforms point-supervised methods including Point2Mask while relying solely on image-level tags. All evaluations were performed on the validation datasets.

Method	Backbone	Supervision	VOC 2012					COCO 2017				
			PQ	PQ th	PQ st	SQ	RQ	PQ	PQ th	PQ st	SQ	RQ
Panoptic FCN [41]	ResNet-50	M	67.9	66.6	92.9	-	-	43.6	49.3	35.0	80.6	52.6
Mask2Former [9]	ResNet-50	M	73.6*	72.6*	93.5*	90.6*	80.5*	51.9	57.7	43.0	-	-
Grounding DINO [49] + SAM [33]	Swin-B	B	48.0*	46.0*	86.7*	84.6*	51.1*	13.3*	20.1*	3.0*	47.3*	15.4*
	Ferret [76] + SAM [33]	LLaMA-13B	B	58.6*	61.6*	79.9*	90.7*	63.8*	13.3*	21.6*	0.8*	45.2*
PSPS [16]	ResNet-50	P	49.8	47.8	89.5	-	-	29.3	29.3	29.4	-	-
Panoptic FCN [41]	ResNet-50	P	48.0	46.2	85.2	-	-	31.2	35.7	24.3	-	-
Point2Mask [40]	ResNet-50	P	53.8	51.9	90.5	-	-	32.4	32.6	32.2	75.1	41.5*
Point2Mask [40]	Swin-L	P	61.0	59.4	93.0	-	-	37.0	37.0	36.9	75.8	47.2
JTSM [62]	ResNet-18-WS	I	39.0	37.1	77.7	-	-	5.3	8.4	0.7	30.8	7.8
MARS [27]	ResNet-50	I	41.4*	39.8*	85.3*	83.0*	57.8*	11.7*	13.3*	10.2*	58.3*	11.8*
+ DiffEGG (Ours)	ResNet-50	I	50.4	48.5	88.9	86.6	60.1	29.5	31.1	28.9	62.5	39.3
DHR [28]	ResNet-50	I	45.0*	43.3*	88.3*	83.3*	59.8*	18.3*	17.5*	18.1*	69.3*	14.8*
+ DiffEGG (Ours)	ResNet-50	I	56.9	55.2	91.0	88.4	63.4	32.8	32.7	32.9	75.5	42.5
+ DiffEGG (Ours)	Swin-L	I	63.9	62.7	94.1	92.5	65.2	37.5	37.8	37.8	76.4	48.1

M: Complete Mask Supervision, B: Box Supervision, P: Point Supervision, I: Image-level Tag (Regardless of Number of Instances)

* Reproduced results using publicly accessible code for a fair comparison. The rest are the values reported in the publication.

models, such as Mask2Former [9], with our WPS masks and evaluate its performance on standard benchmarks (see Appendix E for more details on evaluation metrics including PQ, RQ, and SQ). Remarkably, although existing WPS methods rely on both tag and point annotations [40, 16], our DiffEGG+WSS approach—using only tag annotations without additional point inputs—achieves higher performance (see Table 2). This result validates the efficacy of the proposed DiffEGG refinement.

5.4 Ablation Study

Advanced Backbones & SAM for PS. Our experiments (see Table 2) clearly show that DiffEGG offers strong backbone flexibility. Notably, open-vocabulary panoptic segmentation approaches incorporating SAM [33] (e.g., Grounding DINO [49] + SAM, Ferret [76] + SAM) deliver only marginal gains even with box annotations. In contrast, our class tag-based method (DHR with DiffEGG) achieves superior performance without additional supervision.

Significance of a Diffusion Backbone for Edge Prediction. Feature map visualizations reveal that, unlike DINO or CLIP features, early self-attention maps from diffusion models distinctly capture instance-level details (see Fig. J). These maps, obtained by PeakKL, enable effective edge detection and segmentation enhancement. As shown in Table 3, even the smallest diffusion model (SD1.5 [57]) outperforms larger non-diffusion backbones (e.g., LLaVA-13B [47]), underscoring the advantages of using a diffusion backbone for edge prediction.

5.5 Discussion

Reasoning for Instance Edge Generation. Generating instance edges removes the need for instance-specific hyperparameters (e.g., the maximum instance count as seen in Mask2Former [9]) and enables flexible handling of varying instance numbers (see Appendix A). Moreover, compared to mask generation approaches (i.e., anchor-based methods [9]), edge- and polygon-based approaches [43, 54] are more than four times more computationally efficient. Following two advantages above, we integrate an edge generator with a diffusion backbone. Leveraging the diffusion model’s ability to distinguish adjacent instances, our DiffEGG framework is the first to improve performance in both unsupervised instance segmentation

Table 3: **Comparison of DiffEGG fine-tuning with different backbones.** For a fair comparison, we apply all components (except for PeakKL) to the non-diffusion backbones.

Method	Backbone for DiffEGG	Params. (MB)	COCO 2014		COCO 2017	
			AP^{mk}	AR_{100}^{mk}	AP^{mk}	AR_{100}^{mk}
ProMerge	-	-	3.1	7.6	2.5	7.5
+ DiffEGG	DINOv2-G [52]	1,136	2.6	7.7	2.4	7.2
+ DiffEGG	EVA02-E [18]	5,044	3.2	7.9	2.8	7.8
+ DiffEGG	LLaVA-13B [47]	13,350	3.8	8.4	3.1	8.1
+ DiffEGG	SD1.5 [57]	859	6.8	11.2	5.6	10.1
+ DiffEGG	SDXL [55]	2,567	<u>7.4</u>	<u>12.3</u>	<u>6.0</u>	<u>10.4</u>
+ DiffEGG	SD3.5-L [14]	8,056	8.2	13.1	7.8	11.2

Table 4: **Effect of DiffEGG fine-tuning on Problem A and Problem B.** We split the VOC validation set into images with adjacent instances (Problem A) and those without (Problem B). Fine-tuning with DiffEGG (Stage 1 + Stage 2, see Fig. 4) significantly boosts both AP and AR in both subsets, whereas point annotations yield only minimal improvements relative to their cost.

Method	Problem A		Problem B	
	AP^{mk}	AR_{100}^{mk}	AP^{mk}	AR_{100}^{mk}
MaskCut [67]	3.4	8.5	10.2	23.8
+ Stage 1 (Section 4.2)	4.1 (+0.7)	9.8 (+1.3)	11.2 (+1.0)	24.9 (+1.1)
+ Stage 1 & 2 (Sections 4.2 and 4.3)	6.8 (+3.4)	11.9 (+3.4)	14.3 (+4.1)	30.9 (+7.1)
+ Stage 1 & 2 & Point annotations	6.9 (+3.5)	12.1 (+3.6)	14.5 (+4.3)	31.0 (+7.2)

(UIS) and weakly-supervised panoptic segmentation (WPS).

Quantitative Analysis of Problem A and B. By splitting the VOC validation set into images with adjacent instances (**Problem A** dataset; 49% of the VOC) and those without (**Problem B** dataset; 51% of the VOC), our results (Table 4) show that diffusion fine-tuning markedly enhances both AP and AR in each subset. This indicates that DiffEGG effectively mitigates both *adjacent instance merging* and *single instance fragmentation*. One might question why the absolute AP values remain relatively low; this is due to the initial UIS seed quality from the base model, MaskCut, which provides a weaker starting point for DiffEGG’s enhancement. Additionally, the conceptual analysis of **Problem A** and **Problem B** is provided in Appendix A.

Inference Dynamics in Diffusion Models. Analysis of self-attention maps across diffusion timesteps provides novel insights into the denoising process from a segmentation perspective. In diffusion models, the denoising starts with high-level global structures and transitions to refining local textures and details. Early stages encode key instance-level structure (such as object count and spatial layout), forming a blueprint that guides detailed refinement in later timesteps. This explains why instance-related features are established early stages but become less distinct in later stages as the global structure consolidates. DiffEGG utilizes these early maps for robust instance edge detection, thereby eliminating reliance on manual annotations.

Advantages over DINO-based Approaches. Existing UIS methods [67] typically use self-supervised vision transformers (e.g., DINOv1 [5]). However, unlike diffusion models, DINO variants [52] lack a progressive refinement process and do not train with text prompts specifying object count, leaving them without cues for instance discrimination. Their attention mechanisms and feature maps are tuned for one-shot recognition and classification rather than iteratively refining instance layouts, limiting their capacity to capture instance-level details. The progressive shift of focus paired with instance-specific text prompt conditioning may explain the natural emergence of instance-awareness in self-attention maps of diffusion models.

6 Conclusion

We introduce **DiffEGG**, a novel framework for **Diffusion-driven EdGe Generation** that can be applied to segmentation tasks to resolve adjacent instance merging and single instance fragmentation without requiring pixel-level instance annotations. Looking ahead, DiffEGG’s ability to capture instance features at early timesteps suggests applications beyond segmentation. Our instance-aware edge maps could benefit object tracking, enhancing continuity and accuracy, or medical imaging, where precise boundary identification is essential. Furthermore, DiffEGG’s feature-level instance distinction could expand into video object segmentation, where temporal coherence is key. These directions highlight DiffEGG’s versatility, paving the way for further exploration across diverse fields.

Supplementary Materials

A Limitations of Existing UIS Methods

Our method tackles the root causes of problems. Prob. A stems from UIS methods [67] relying on semantic backbones [5], lacking instance-level distinction. We resolve this using instance-aware diffusion self-attention maps via PeakKL/EdgeKL. Prob. B arises from fixed hyperparameters (τ , n) in graph-cut methods [67], leading to inconsistent granularity. We resolve these issues via non-parametric instance edge & RIP. Along with Table 4, Figs. K, O and P provide qualitative validation. Appendix A and Table E give detailed analysis.

A.1 Problem A. Adjacent Instance Merging

Root Cause of Problem A: Limitations of Existing Backbones. UIS methods [51, 68, 67, 36] depend on pretrained "backbones" (e.g., DINO [5]) to extract feature maps, which are subsequently partitioned into instance masks through techniques like graph cut [69]. However, these backbones were originally designed to distill information primarily about *semantic* segmentation—identifying and classifying foreground objects from the background, rather than distinguishing individual instances within a class. This inherent design limitation makes it difficult to achieve true instance separation (e.g., distinguishing two adjacent boats in the top of Fig. G) using only semantic features.

MLLM Backbones Share This Limitation, and More Parameters Do Not Resolve It. When prompted with "Describe this image" in Fig. J, LLaVA-13B’s self-attention maps only capture semantic features, while diffusion models (e.g., SD1.5) separate instances, a capability absent in other foundation models. In Table 3, diffusion backbones substantially outperform CLIP/DINO/MLLM counterparts with comparable/fewer parameters.

Our Solution for Problem A. To overcome the limitations of semantic-oriented backbones, we introduce DiffEGG, a framework that leverages the inherent spatial attention in diffusion models to generate instance-aware edges without requiring pixel-level annotations. DiffEGG harnesses self-attention maps from pretrained diffusion models, which capture instance boundaries through attention mechanisms tuned during pretraining. By introducing two novel metrics, PeakKL and EdgeKL, DiffEGG autonomously identifies and reinforces instance boundaries, ensuring that adjacent instances are effectively separated, even when traditional feature maps fall short. Unlike conventional UIS methods [51, 68, 67, 36] that rely on semantic segmentation backbones, DiffEGG uses a self-supervised fine-tuning step that enhances edge connectivity, achieving precise instance delineation across classes. This enables DiffEGG to address the issue of adjacent object merging by focusing specifically on instance edges, demonstrating superior separation accuracy across challenging datasets (e.g., VOC [15], COCO [44]), as shown in our experimental results (see Table 1 and Table 2). Our diffusion-based approach addresses the adjacency issue by focusing on instance-level edge generation rather than relying solely on semantic features, making it a scalable solution for UIS.

A.2 Problem B. Single Instance Fragmentation

Root Cause of Problem B: Limitations of Graph Cut. Graph-cut based UIS methods [69, 67, 36] require a hyperparameter, τ , which acts as a threshold for the initial graph construction. In this approach, the image is represented as a graph, where each pixel (or patch) corresponds to a vertex, and each edge represents the degree of similarity (i.e., affinity) between two pixels (or patches). The affinity $A_{i,j}$ between vertices i and j is measured using the cosine similarity $\mathcal{S}_{i,j}$ of their respective feature maps. If $\mathcal{S}_{i,j} \geq \tau$, vertices i and j are connected by an edge; otherwise, they are not connected.

Intuitively, τ determines the sensitivity of the UIS method to similarities between feature maps. For instance, if τ is close to 1, only pixels with nearly identical feature maps are considered connected. Conversely, if $\tau = 0$, every pixel is connected to every other pixel. The graph-cut algorithm then partitions the graph into two partitions—a foreground partition and a background partition—by minimizing the number of edges that need to be removed. The foreground object is identified using a heuristic rule, and the corresponding partition is presented as an instance mask. For the UIS method to detect at most n distinct instances, this process needs to be repeated for n iterations, where n is a fixed hyperparameter.

The value of τ impacts the granularity of the instance masks produced by graph-cut based methods (see Fig. H). A fixed τ often leads to fragmentation of single instances or merging of multiple instances,

Component	Main Role	Contributions to Problem A	Contributions to Problem B
PeakKL	Finds optimal step for instance boundaries	Separates adjacent instances in feature space	Provides initial edge information for merging
EdgeKL	Converts self-attention maps to edge maps	Detects edge seeds between adjacent instances	Provides instance-aware edge maps for merging
Fine-tuning	Enhances connectivity in edge maps	Completes edges between adjacent instances	Refines instance edges to resolve fragmentation
RIP	Instance-aware random walk propagation	Separates instances using refined edges	Propagates and merges fragmented instance masks

Table E: **Component contributions to solve (A) adjacent instance merging and (B) single instance fragmentation.** Each step builds on the previous one, with RIP finalizing adjacent instance separation and fragmentation resolution using the refined edges generated by PeakKL, EdgeKL, and fine-tuning.

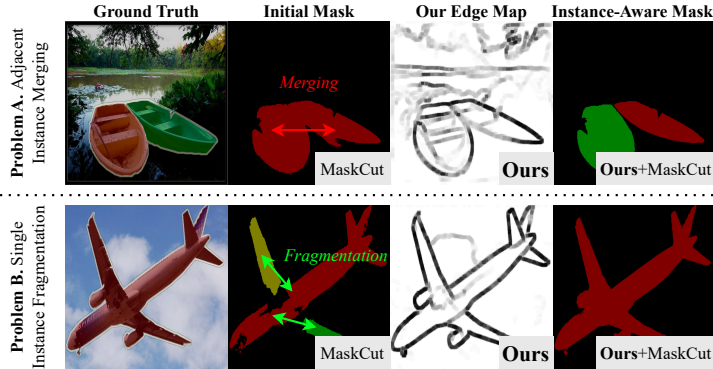


Figure G: **Additional examples of problem A and B and our solution.**

as it cannot be dynamically adjusted for each image. Additionally, methods that fix iteration counts, n , cannot detect more than n instances, failing in instance-dense images. This fixed tuning for τ and n may work on the average case, but does not generalize well across different images.

Our Solution for Problem B. By contrast, DiffEGG predicts edges between adjacent instances without tuning hyperparameters (e.g., n , τ) related to instance count, making it more flexible and robust. Experimentally, DiffEGG-generated edges effectively resolve fragmentation and separate adjacent instances, achieving both conceptual and practical advantages. Since DiffEGG-generated edges accurately delineate each instance, we can use the edge map to construct a transition probability matrix for a random walk on the pixel space. This spreads out the masks within the edges (increased IoU between masks of the same instance) while effectively stopping masks from spreading over the edges (restricted IoU between masks of distinct instances, even if the instances are adjacent). As a result, our **edge-generation approach** allows DiffEGG to handle both adjacent instance merging and single instance fragmentation, enhancing existing UIS methods [36, 67].

B Comprehensive Review of Related Work

B.1 Instance Segmentation

Instance segmentation (IS) aims to delineate and label individual object instances within images. Traditional IS approaches rely on pixel-level annotations, which can be resource-intensive, particularly for large datasets. More recent work has expanded into unsupervised methods to address scalability concerns. Meanwhile, panoptic segmentation (PS) methods, designed to handle both semantic and instance segmentation in a unified task, often serve as competitive baselines for instance segmentation capabilities. Panoptic models distinguish between "things" (countable objects) and "stuff" (amorphous regions) and can separate multiple instances of the same class. Here, we categorize recent IS and PS methods based on their reliance on annotations.

Fully-supervised Segmentation. Many established methods [9, 42, 78, 8, 41, 32, 73], such as Mask2Former [9] and Panoptic SegFormer [42], require dense, pixel-level annotations (i.e., masks) to achieve accurate instance segmentation but face scalability issues due to high annotation costs. These models are designed for panoptic segmentation, but serve as baselines for instance segmentation. We refer to these methods as "panoptic models".

Point/Box-Supervised Segmentation. These weakly-supervised methods [40, 16, 38, 39, 25] aim to reduce annotation costs by using less detailed - but instance-specific - labels like points or boxes

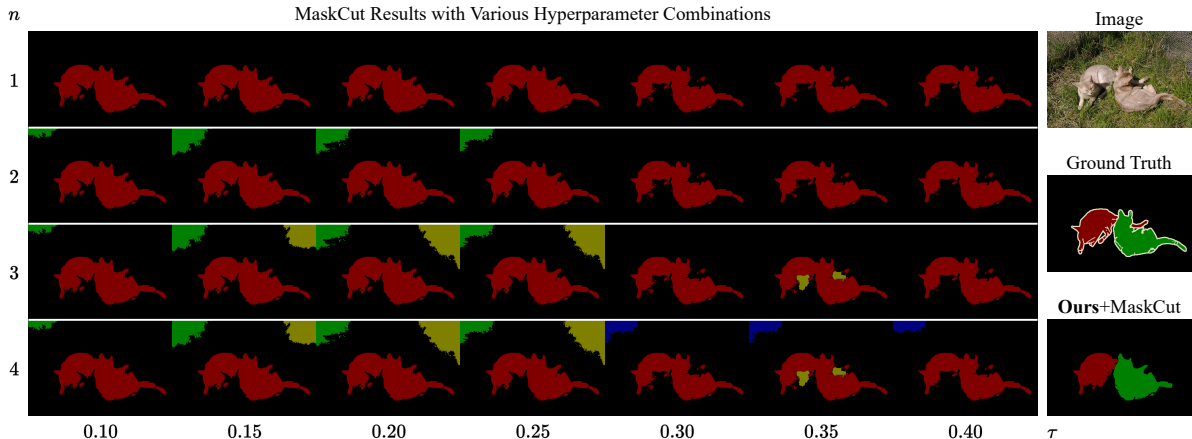


Figure H: **Drawbacks of MaskCut with various n, τ combinations.** Due to the semantic-oriented nature of the DINO backbone used in MaskCut, increasing n or decreasing τ does not result in the successful separation of the two adjacent instances. Rather, changing the hyperparameters leads to fragmentation and detection of false positives in the background.

for each instance. These methods [40, 16] typically operate in two stages: first, they generate pseudo-panoptic masks from weak annotations, and then a panoptic model (e.g., Mask2Former) is trained using these pseudo-masks instead of ground-truth annotations. Although annotation effort is reduced, the reliance on manual points and boxes still presents a substantial cost. However, DiffEGG is annotation free.

Tag-Supervised Segmentation. Tag-supervised instance segmentation uses image-level tags (e.g., "person") without any instance-level details (e.g., location of each person). While only a single image-level tag is required per image, depending on the number of instances, multiple instance-level annotations may be required. Hence, tag supervision is significantly cheaper than instance-level annotations.

- **Instance Segmentation with Class Activation Maps (CAM) [79].** CAM-based instance segmentation methods [30, 81] leverage heatmap and class tags for rough localization of class-related regions. However, CAM was initially designed for semantic segmentation, and its lack of precision in localizing specific instances limits its effectiveness for instance-level segmentation (see Appendix for details).
- **Weakly-supervised Semantic Segmentation (WSS).** WSS methods [29, 58, 31, 35, 12, 75, 27, 82, 46, 60, 26, 74, 37, 48, 7, 72, 17] use image-level tags or captions and offer promising results in class-level segmentation. However, WSS alone cannot produce instance-level masks without further refinement. DiffEGG provides the instance-level refinement that can extend WSS methods to tag-supervised PS methods.

We note that the use of class tags is the minimal possible annotation which allows models to focus on specific classes in an image, crucial for evaluating performance in PS tasks. Methods that do not incorporate class tags (e.g., U2Seg [51]) are excluded from our comparisons with PS methods, as they cannot produce specific class labels. U2Seg attempts unsupervised panoptic segmentation by combining MaskCut [67] for unsupervised instance segmentation with STEGO [21] for unsupervised semantic segmentation. However, without tag-supervision, U2Seg cannot generate correct class labels, generating labels such as "class 1" instead of "cat 1", which restricts its applicability. Some methods, like JTSM[62], use class tags but demonstrate limited PS performance, further indicating a gap in this domain. Remarkably, DiffEGG+WSS, which uses only tag-supervision in the WSS method, outperforms methods using point supervision.

Unsupervised Instance Segmentation (UIS). UIS aims to perform instance segmentation without relying on any annotations. Existing UIS methods can be broadly categorized based on their architectural foundation: DINO-based methods [51, 68, 67, 36] like MaskCut [67] and ProMerge [36] apply feature clustering with the graph cut algorithm on pretrained self-supervised vision transformer (i.e., DINO [5]) backbones to separate instances. SOLO-based approaches [66, 24] rely on CNN-based (e.g., DenseCL [65]) pseudo-mask generation but show poor performance and requires training from scratch,

making them computationally expensive. UIS serves as a direct baseline for DiffEGG, as these methods attempt instance separation without any labels.

DiffEGG stands out from existing instance segmentation literature by taking a fully unsupervised, edge-oriented approach instead of clustering features via graph cut. Also, instead of DINO or SOLO-based backbones, DiffEGG leverages a generative diffusion model.

B.2 Diffusion Models in Segmentation

Text-to-image diffusion models [53, 3, 14, 55] are trained on image-caption pairs to learn complex visual-text relationships, with recent versions such as SDXL [55] and SD3 [14] offering finer control through transformer-based architectures. These models generate refined images by iteratively denoising latent representations, making them effective for detailed image synthesis. Recently, diffusion models have shown potential for segmentation tasks by generating pseudo-masks and aiding unsupervised segmentation. Relevant methods include:

- **Diffusion-based Segmentation Methods.** DiffCut [11] and DiffSeg [64] use clustering on self-attention maps for semantic segmentation. DiffCut generates pixel-groupings by clustering diffusion model embeddings with Normalized Cuts, but requires careful tuning of the clustering threshold for optimal results. DiffSeg, on the other hand, extracts semantic regions directly from self-attention layers, but DiffSeg’s masks lack fine instance details. These methods aim at semantic segmentation, and cannot be extended to instance segmentation.
- **Synthetic Dataset Generation.** DatasetDM [70] and Dataset Diffusion [50] synthesize image segmentation datasets via diffusion. While effective for creating varied, annotated datasets, these models cannot be directly applied to real-world datasets and therefore have limited utility for practical segmentation tasks.

Existing diffusion-based segmentation methods [11, 64] focus on later timesteps in the inversion process, when image structures are nearly complete. However, this focus limits their ability to identify and separate multiple instances, as instance-specific information appears in the early timesteps but fades as the model builds the overall semantic structure. This novel use of early diffusion features enables DiffEGG to capture instance-level information and perform instance segmentation effectively.

C Method Details

C.1 Self-Attention Accumulation

For a noised image X_t at time step t , the self-attention mechanism computes spatial dependencies using weights W_Q, W_K :

$$Q_t = X_t W_Q, K_t = X_t W_K \in \mathbb{R}^{HW \times d} \quad (9)$$

$$SA(X_t) = \text{softmax} \left(\frac{Q_t K_t^T}{\sqrt{d}} \right) \in [0, 1]^{HW \times HW} \quad (10)$$

where d is the dimensionality of the attention heads, and H, W are the height and width of the self-attention map.

In text-to-image diffusion models, multiple self-attention maps SA_1, \dots, SA_N are produced at various resolutions w_1, \dots, w_N (w_i is the width of the i th SA map). We accumulate these maps by upsampling each to the resolution of the highest-resolution map, followed by averaging across all maps:

$$SA[i, j, :, :] = \frac{1}{N} \sum_{k=1}^N SA_k \left[\frac{i}{\delta_k}, \frac{j}{\delta_k}, :, : \right] \quad (11)$$

$$\delta_k = \frac{\max_{1 \leq j \leq N} w_j}{w_k} \quad (12)$$

The hooker function $\mathcal{H}(\epsilon_\theta, X_0, t)$ (see Section 3.2) extracts all self-attention maps evaluated in the forward pass at timestep t given input image X_0 and returns the accumulated attention map (11).

Table F: **Computational overhead and alternative edge metrics in DiffEGG (SDXL backbone), evaluated on a single A100 GPU.**

Phase (Dataset)	MaskCut [67]	DiffEGG	Edge{Metric}	Latency/img	AP^{mk}
Training (ImageNet)	-	8 days	KL (Ours)	600ms	9.4
Inference (VOC2012)	4.5 hours	+ 0.1 hours	JSD	615ms	9.2
Inference (COCO2014)	36 hours	+ 2 hours	L2	425ms	6.8
VRAM of DiffEGG: 34GB (Train.) & 20GB (Infer.)			Cosine	2,700ms	8.3

C.2 PeakKL and EdgeKL Algorithms

Algorithm 1 (PeakKL, Section 4.1): Identifies the optimal diffusion timestep for instance separation by finding the timestep with peak KL-gap.

Algorithm 1 PeakKL : X_0 (Image) \mapsto SA_{inst}

Require: Image X_0

Sequence of timesteps $\tau_1 > \tau_2 > \dots > \tau_N$

Frozen Text-to-Image Diffusion Model $\epsilon_{\theta^*}(\cdot, \cdot)$

```

1: Initialize:  $KL\text{-gap} \leftarrow 0$ ,  $SA_{inst} \leftarrow \emptyset$ 
2:  $\hat{X}_0 \leftarrow \text{Reconstruct}(\epsilon_{\theta^*}, X_0, \tau_1)$  Hook  $\mathcal{H}$ 
3:  $SA[1] \leftarrow \mathcal{H}(\epsilon_{\theta^*}, X[0], \tau_1)$ 
4: for  $n = 2$  to  $N$  do
5:    $\hat{X}_0 \leftarrow \text{Reconstruct}(\epsilon_{\theta^*}, X_0, \tau_n)$  Hook  $\mathcal{H}$ 
6:    $SA[n] \leftarrow \mathcal{H}(\epsilon_{\theta^*}, X_0, \tau_n)$ 
7:   if  $KL\text{-gap} < D_{KL}(SA[n] \parallel SA[n-1])$  then
8:      $KL\text{-gap} \leftarrow D_{KL}(SA[n] \parallel SA[n-1])$ 
9:      $SA_{inst} \leftarrow$  normalized  $SA[n]$ 
10:  end if
11: end for
12: return  $SA_{inst}$ 

```

Algorithm 2 (EdgeKL, Section 4.2): Transforms self-attention maps into edge maps, allowing instance-aware boundary detection without annotations. For any given image of resolution 1024×1024 , EdgeKL computation takes 800ms on average on a single A100 GPU. Among various metrics tested for computing edges in (6), KL achieves the best accuracy-efficiency trade-off in Table F(right).

Algorithm 2 EdgeKL: $SA_{inst} \mapsto E$ (Pseudo-Edge)

Require: Self-Attention Map SA_{inst}

```

1: Initialize:  $E_0 \leftarrow \mathbf{0}_{H \times W}$ 
2: for  $(i, j)$  in  $[H] \times [W]$  do
3:    $E_0[i, j] \leftarrow \text{EdgeKL}(i, j; SA_{inst})$ 
4: end for
5:  $\mu \leftarrow$  mean of  $E_0$ 
6:  $\sigma \leftarrow$  standard deviation of  $E_0$ 
7:  $E = \begin{cases} \mathbf{1} \cdot [E_0 > \mu + \sigma] & \text{Edge Pixel} \\ \mathbf{0} \cdot [E_0 < \mu - \sigma] & \text{Interior Pixel} \\ (-\mathbf{1}) \cdot [\text{otherwise}] & \text{Uncertain Pixel} \end{cases}$ 
8: return  $E$ 

```

C.3 Fine-tuning Algorithm

Algorithm 3 (Fine-tuning, Section 4.3): Fine-tunes the transformer layers of text-to-image diffusion models and trains a new edge generator \mathcal{G}_ϕ from scratch. For the architecture of \mathcal{G}_ϕ , we follow [71] and utilize a Feature Pyramid Network (FPN) followed by a Convolutional Neural Network (CNN).

Algorithm 3 DiffEGG Fine-tuning

Require: Image Dataset \mathcal{I} , Pseudo-Edge Set $\{E_I\}_{I \in \mathcal{I}}$ Edge Generator \mathcal{G}_ϕ Pretrained Text-to-Image Diffusion Model ϵ_θ 1: **for** Epoch in $1 \dots N$ **do**2: $\mathcal{L} \leftarrow 0$ 3: **for** I in \mathcal{I} **do**4: $\hat{I} \leftarrow \text{Reconstruct}(\epsilon_\theta, I, \tau = 0)$ 5: $\hat{E} \leftarrow \mathcal{G}_\phi(\mathcal{H}(\epsilon_\theta, I, \tau = 0))$ 6: $E \leftarrow E_I$ 7: $\mathcal{L} \leftarrow \mathcal{L} + \|I - \hat{I}\|^2 + \text{DiceLoss}(E, \hat{E})$ 8: **end for**9: Backprop on $\mathcal{L}(\theta, \phi)$ 10: **end for**

Hook \mathcal{H}
Predicted Edge
Pseudo-Edge

C.4 Random-Walk Instance Propagation (RIP)

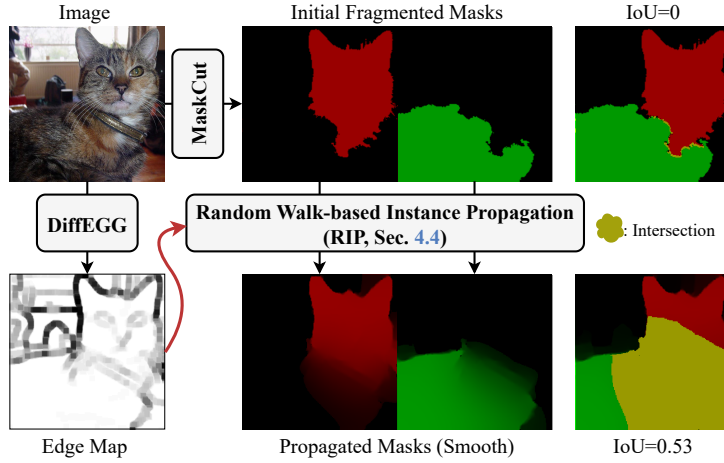


Figure I: **Random walk-based instance propagation (RIP)**. Our DiffEGG-generated edge map can be used to define transition probabilities on a given instance mask such that fragmented masks are spread out within the boundaries of its instance. The yellow regions indicate the intersection between the two masks.

Algorithm 4 UIS/WSS + DiffEGG

Require: Image I Trained Edge Generator \mathcal{G}_{ϕ^*} Fine-Tuned Diffusion Model ϵ_{θ^*} Masks M_1, \dots, M_N from a UIS/WSS Method1: $\hat{I} \leftarrow \text{Reconstruct}(\epsilon_{\theta^*}, I, \tau = 0)$ 2: $\hat{E} \leftarrow \mathcal{G}_{\phi^*}(\mathcal{H}(\epsilon_{\theta^*}, I, \tau = 0))$ 3: Identify Connected Components with \hat{E} and CCL4: $\mathcal{A} \leftarrow \text{Affinity}(\hat{E})$ 5: $T = D^{-1} \mathcal{A}^{\alpha\beta}$, $D_{ii} = \sum_j \mathcal{A}_{ij}^\beta$ 6: $\text{vec}(M_n^*) = T^t \cdot \text{vec}(M_n \odot (1 - \hat{E}))$

7: Merge Masks

8: Return Final Masks

Hook \mathcal{H}
Predicted Edge $\forall n = 1 \dots N$

We apply the random walk propagation methods proposed in [2, 1]. Here, we outline a high-level overview of the propagation technique.

Table G: **Unsupervised instance segmentation (UIS) performance comparison on multiple benchmarks.** We compare TokenCut, MaskCut, ProMerge, re-implemented for a fair comparison with DiffEGG. DiffEGG is set up with the SD3.5-L backbone and uses initial instance masks generated by ProMerge. To ensure a fair comparison with existing UIS models fine-tuned on ImageNet [34], we also fine-tune our diffusion model and edge generator on ImageNet. This allows us to generate DiffEGG-based instance edges from the ImageNet-trained model and apply them directly to other datasets (e.g., VOC2012 [15], COCO2014 [44]) without further fine-tuning.

Method	VOC 2012		COCO 2014		COCO 2017		LVIS		KITTI		Objects365		SA-1B		Average	
	AP ^{mk}	AR ^{mk} ₁₀₀														
TokenCut [69]	6.1*	10.6*	2.7	4.6	2.0	4.4	0.9	1.8	0.3	1.5	1.1	2.1	1.0	0.3	2.0	3.6
MaskCut [67]	5.8*	14.0*	3.0*	6.7*	2.3*	6.5*	0.9*	2.6*	0.2*	1.9*	1.7*	4.0*	0.8*	0.6*	2.1	5.2
ProMerge [36]	5.0*	13.9*	3.1*	7.6*	2.5*	7.5*	1.1*	3.4*	0.2*	1.6*	2.2*	6.1*	1.2*	0.8*	2.2	5.8
ProMerge [36] + DiffEGG	9.4	18.2	8.2	13.1	7.8	11.2	2.5	4.7	1.2	2.6	4.3	9.5	2.0	1.6	5.1	8.7

* Reproduced results using publicly accessible code for a fair comparison. The rest are the values reported in the publication.

- Sparse Affinity Construction:** From a pseudo-edge map \hat{E} , construct sparse affinity matrix A_{sparse} by calculating affinities between each pixel and its neighbors along predefined paths. Paths with edges (indicating boundaries) have low affinities, while edge-free paths have affinities closer to 1.
- Sparse to Dense Affinity:** Convert A_{sparse} into a dense matrix A_{dense} by filling in affinities for every pixel pair. For symmetric consistency, if a path exists between pixels i and j , then both $A_{\text{dense}}[i, j]$ and $A_{\text{dense}}[j, i]$ are assigned the same value.
- Seed Propagation:** Compute the transition matrix $T = D^{-1}A_{\text{dense}}^{\circ\beta}$, where D normalizes rows of $A_{\text{dense}}^{\circ\beta}$. After t iterations, updated masks are generated via:

$$\text{vec}(M_c^*) = T^t \cdot \text{vec}(M_c \odot (1 - \hat{E})), \quad (18)$$

where $(1 - \hat{E})$ prevents edge pixels from influencing neighbors, focusing propagation on non-edge regions.

This method creates more coherent and complete instance masks.

C.5 Complexity of DiffEGG

In Table F(left), our fine-tuning (Section 4) enables one-step edge inference (190ms/img). PeakKL-EdgeKL (3s-0.6s/img) are used once during training for initial edges. DiffEGG incurs a 2% overhead [67] for UIS inference and no extra time for WPS inference, as our edge maps generate panoptic masks during training only.

D Additional Experiments

We provide additional experiments that compare ProMerge with DiffEGG(SD3.5-L) (Ours) to TokenCut [69], MaskCut [67], ProMerge [36]. Following public checkpoints, we strictly reproduce three UIS methods [69, 67, 36] for a fair comparison. Total of seven benchmarks—COCO2014 [44] and COCO2017 [4], LVIS [20], KITTI [19], Objects365 [61], and SA-1B [33]—are used. See Appendix E for evaluation specifications. Table G shows an overall 2.3× improvement in instance segmentation performance measured by AP, demonstrating the impact of refined edges in achieving more precise instance segmentation.

E Datasets and Metrics for Evaluation

Datasets for UIS Evaluation. We evaluate our DiffEGG on seven benchmarks including COCO2014 [44] and COCO2017 [4], LVIS [20], KITTI [19], Objects365 [61], and SA-1B [33].

COCO2014 [44] and COCO2017 [4] are standard datasets for object detection and segmentation. COCO2014 has 80 classes, 83K training images and 41K validation images. COCO2017 is composed of 118K and 5K images for training and validation splits respectively. For results on COCO2014 and COCO2017, we use the images in the validation split.

LVIS has densely-annotated instance masks, making it more challenging for segmentation. We test our performance on the validation set containing 245K instances on 20K images. For KITTI and Objects365, we evaluate on 7K images and a subset of 44K images in the val split, respectively. Lastly, for SA-1B, we assess on a subset of 11K images, which come with 100+ annotations per image on average.

Datasets for WPS Evaluation. Pascal VOC [15] consists of 20 "thing" and 1 "stuff" categories. It contains 11K images for training and 1.4K images for validation. COCO2017 [4] has 80 "thing" and 53 "stuff" categories, which is a challenging benchmark for PS. We validate DiffEGG on the 5K images in the validation dataset.

Evaluation Metrics for IS. We evaluate the performance comparison of UIS methods with and without DiffEGG based on average precision (AP) and average recall (AR) on Pascal VOC and MS COCO dataset. Precision and Recall are defined as

$$\text{Precision} = \frac{\text{TP}}{\text{TP} + \text{FP}}, \text{ Recall} = \frac{\text{TP}}{\text{TP} + \text{FN}} \quad (14)$$

where TP, FN, FP are short for True Positive, False Negative, and False Positive, respectively. Intuitively, a high precision means the method has a low rate of making false positives, but it does not imply that all the positives were found. A high recall means the method has a low rate of making false negatives.

AP measures the precision across different recall levels. A high AP means the method finds most objects(recall) while minimizing false positives (precision). On COCO, AP is calculated over different IoU thresholds (0.5, 0.75) and object sizes, then averaged. For Pascal VOC, mAP is used, averaging AP across classes at a single IoU threshold (0.5). COCO uses mAP@IoU=0.5:0.95, meaning it averages AP across ten IoU thresholds(0.50, 0.55, ..., 0.95).

$$AP = \int_0^1 \text{precision}(r)dr \quad (15)$$

$$mAP_{\text{COCO}} = \frac{mAP_{0.50} + mAP_{0.55} + \dots + mAP_{0.95}}{10} \quad (16)$$

Average Recall (AR) is calculated as the area under the recall-threshold curve. Like AP, it is averaged over multiple IoU thresholds. AR reflects how well the method recalls true objects rather than balancing precision and recall. In COCO, AR is reported as AR@100, AR@100 (small), AR@100 (medium), and AR@100 (large), corresponding to the average recall with up to 100 detections per image across different object sizes.

Evaluation Metrics for PS. We report evaluation results on the standard evaluation metrics of panoptic segmentation task, including panoptic quality (PQ), segmentation quality (SQ) and recognition quality (RQ). PQ is defined for matched segments (IoU > 0.5 between predicted and ground truth masks) and combines SQ and RQ:

$$PQ = \frac{\sum_{(p,gt) \in TP} \text{IoU}(p, gt)}{|TP| + 0.5|FP| + 0.5|FN|} \quad (17)$$

Segmentation quality (SQ) measures the accuracy of segment boundaries, focusing only on segments that were correctly identified and ignoring false positives and false negatives. SQ is defined as:

$$SQ = \frac{\sum_{(p,gt) \in TP} \text{IoU}(p, gt)}{|TP|} \quad (18)$$

Recognition quality (RQ) measures the model's ability to correctly classify instances, accounting for both precision and recall for detected instances. RQ combines recall (finding all objects) with precision (only detecting true objects), focusing on instance recognition rather than segmentation quality. RQ is defined as:

$$RQ = \frac{|TP|}{|TP| + 0.5|FP| + 0.5|FN|} \quad (19)$$

Metric	Intuitive Meaning
AP	Balance between precision and recall
AR	Ability to recall true objects
PQ	Combined segmentation quality and recognition quality
SQ	Accuracy of segmentation shapes
RQ	Correct classification of instances

Table H: **Evaluation Metrics on Pascal VOC and COCO datasets.**

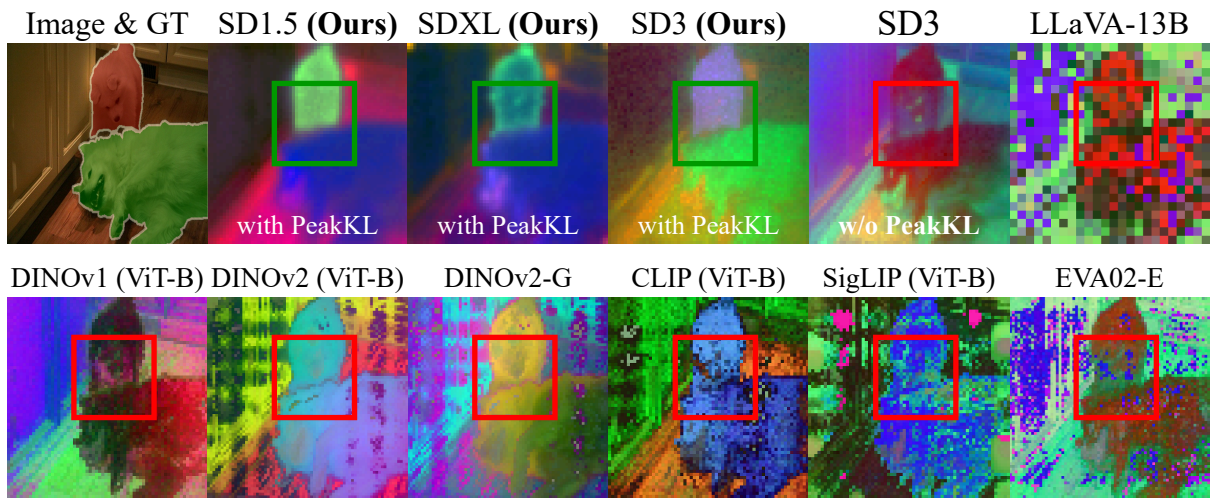


Figure J: **Importance of PeakKL in diffusion-agnostic instance-aware feature map extraction.** PeakKL can extract instance-aware feature maps from various text-to-image diffusion models: SD3 [14] and SDXL [55]. Notice how the Diffusion+PeakKL feature maps uniquely highlight the distinct colors of the two dogs. In contrast, other backbones or diffusion timesteps show the dogs with similar colors, reflecting only semantic-level awareness. While MLLMs/ViTs struggle to distinguish instances (red), Diffusion+PeakKL features (green) are the only ones capable of distinguishing adjacent instances. All feature maps are visualized using PCA, where similar colors represent similar feature maps.

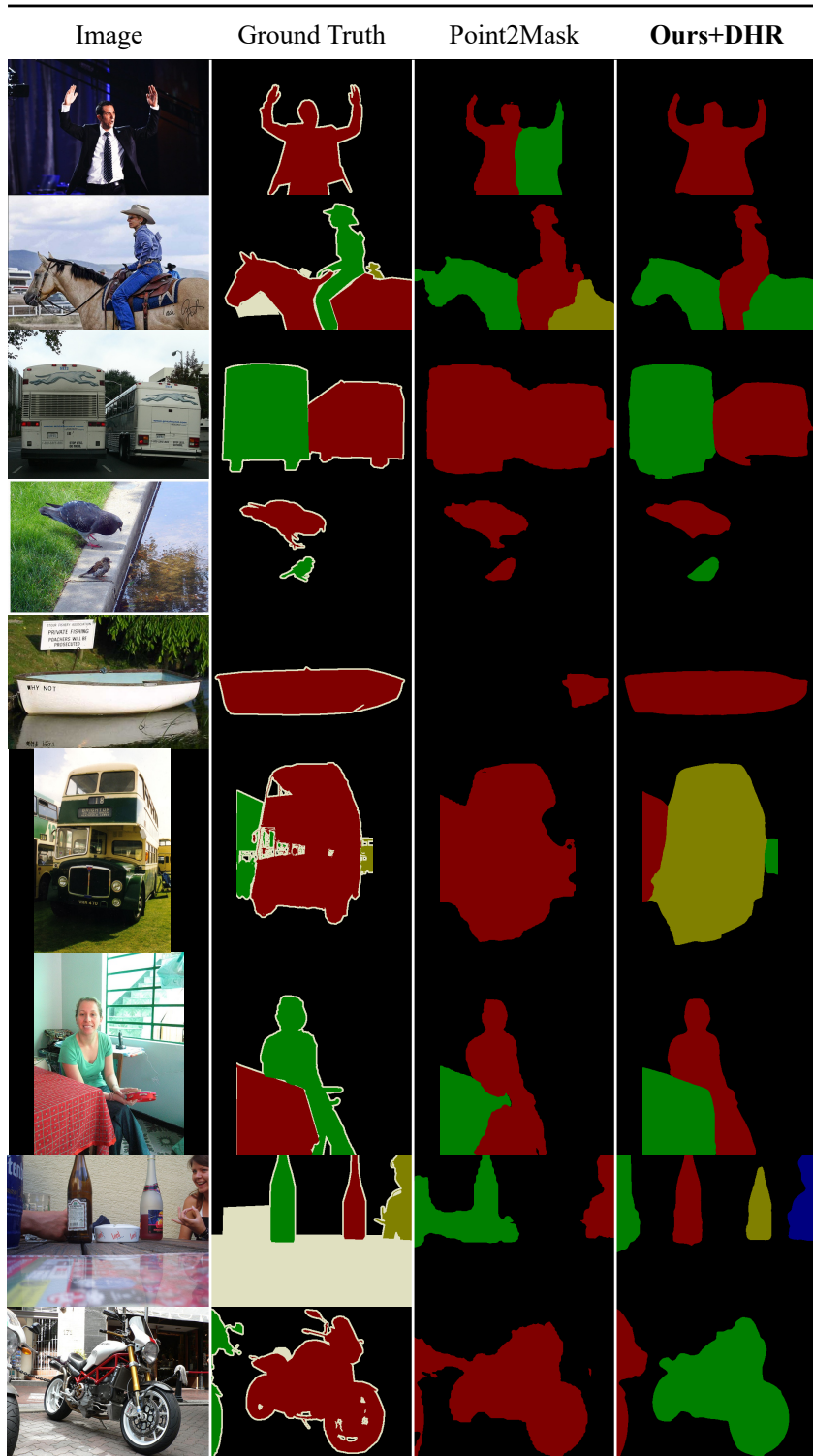


Figure K: Qualitative results in WPS with ours (DiffEGG+DHR [28]) and point-supervised Point2Mask [40] on the VOC2012 [15] validation set. (Ours) We trained a Mask2Former using a ResNet-50 backbone with pseudo panoptic masks generated from DiffEGG+DHR. The samples in this figure are the outputs from Mask2Former trained with our masks.

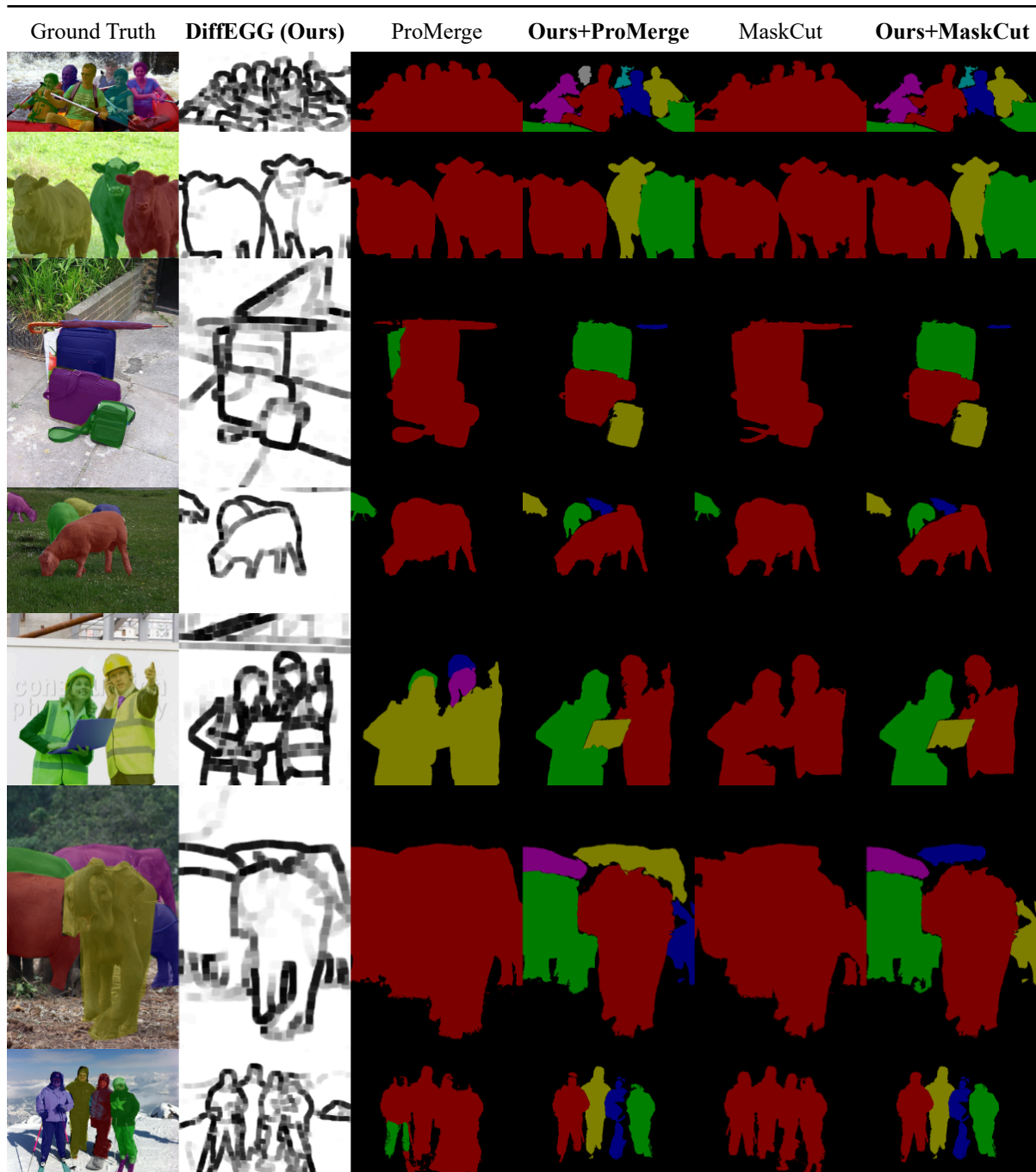


Figure L: Qualitative results in UIS with ours (DiffEGG+ProMerge, DiffEGG+MaskCut) and existing methods (ProMerge [36], MaskCut [67]) on the COCO2014 [45] validation set.

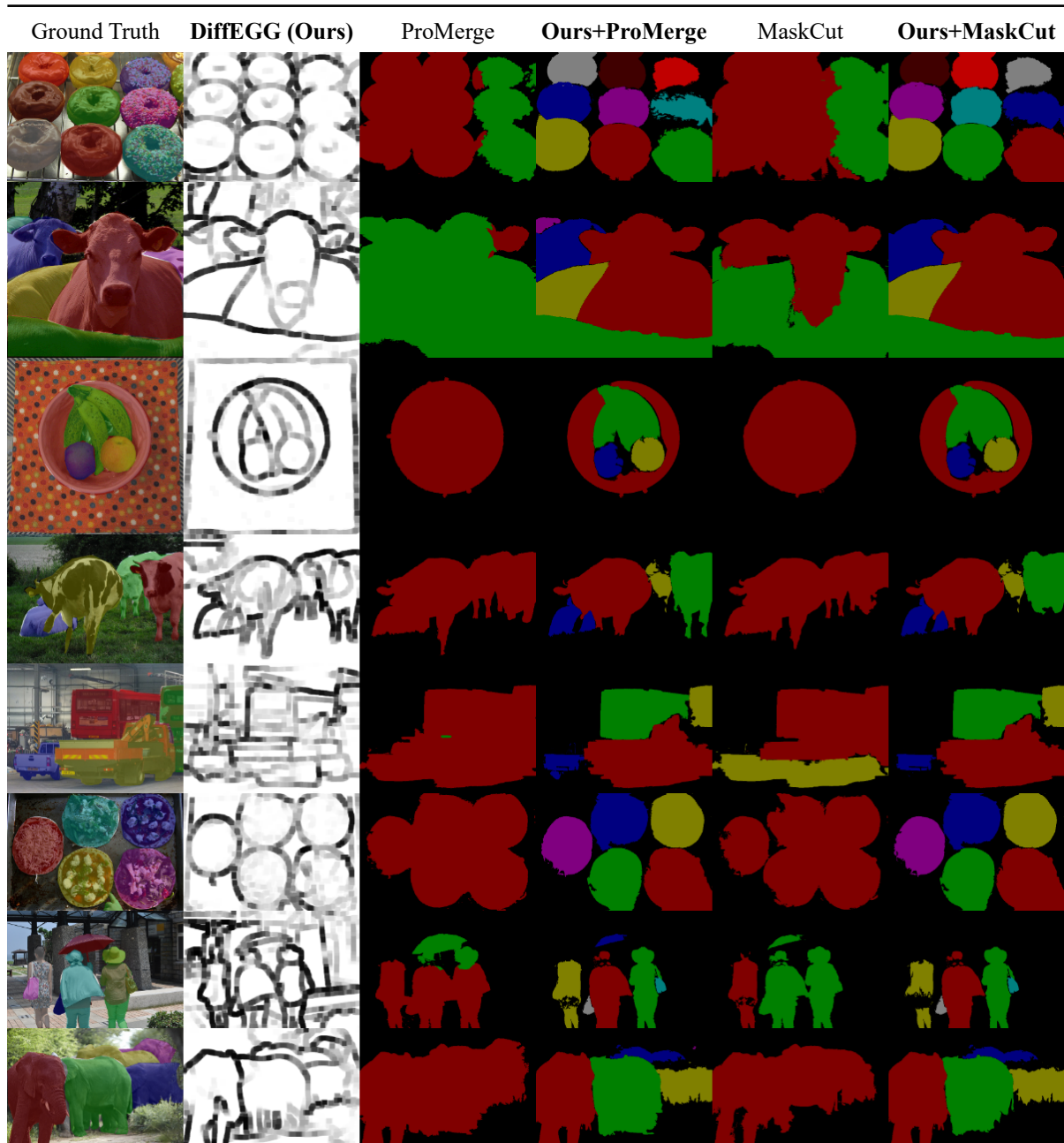


Figure M: More Qualitative results in UIS with ours (DiffEGG+ProMerge, DiffEGG+MaskCut) and existing methods (ProMerge [36], MaskCut [67]) on the COCO2014 [45] validation set.

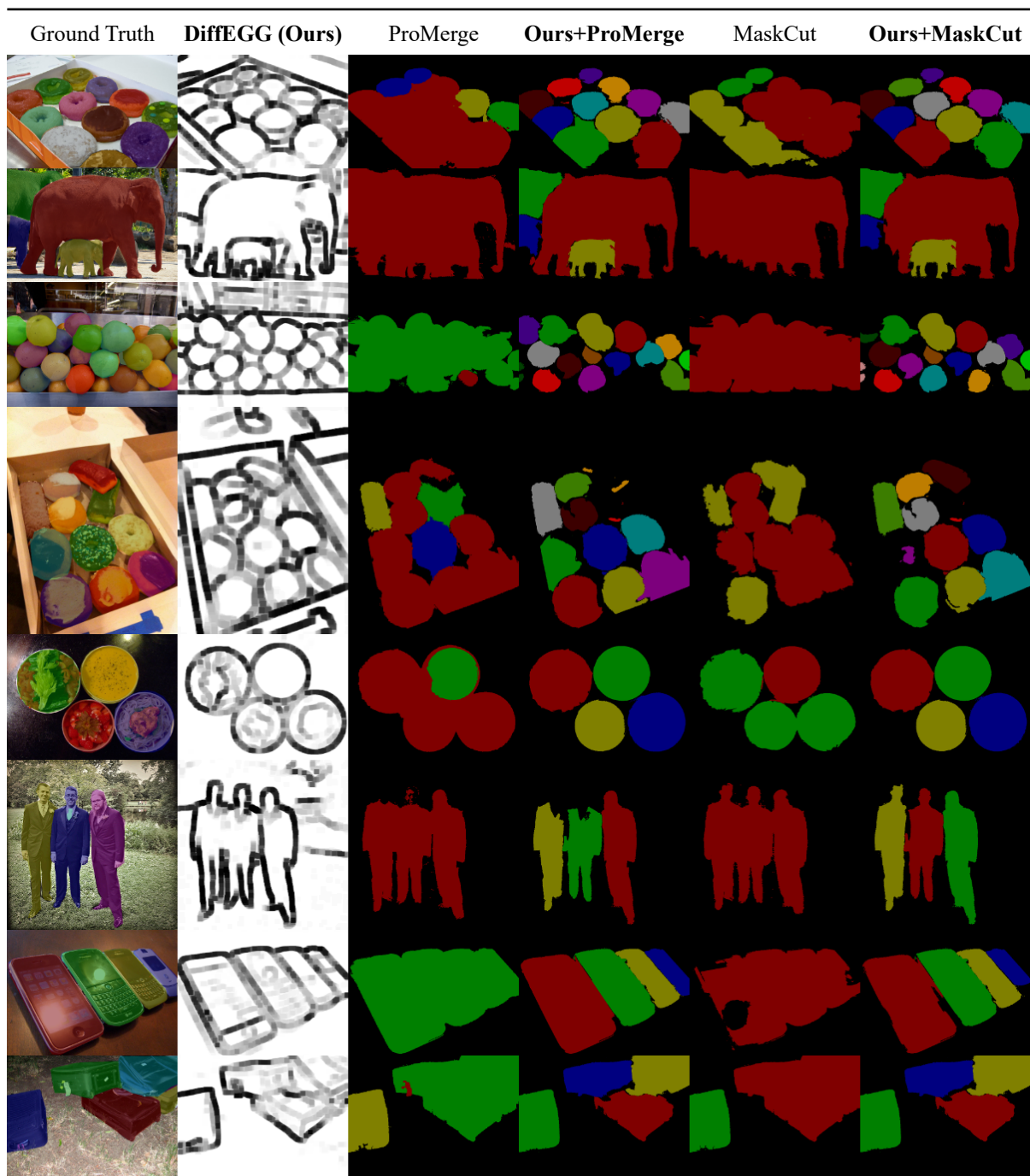


Figure N: More Qualitative results in UIS with ours (DiffEGG+ProMerge, DiffEGG+MaskCut) and existing methods (ProMerge [36], MaskCut [67]) on the COCO2014 [45] validation set.

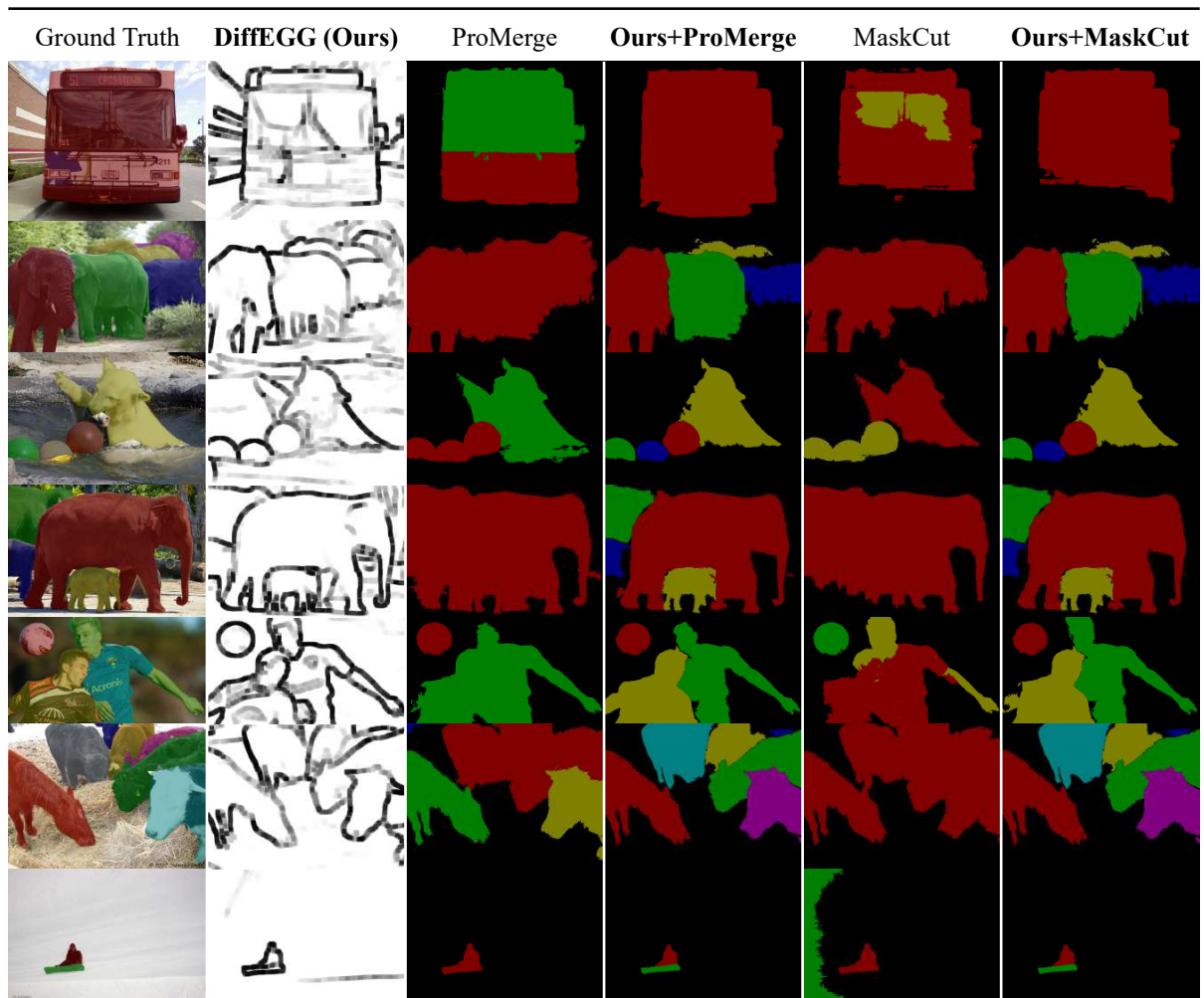


Figure O: Qualitative results in UIS with ours (DiffEGG+ProMerge, DiffEGG+MaskCut) and existing methods (ProMerge [36], MaskCut [67]) on the COCO2017 [4] validation set.

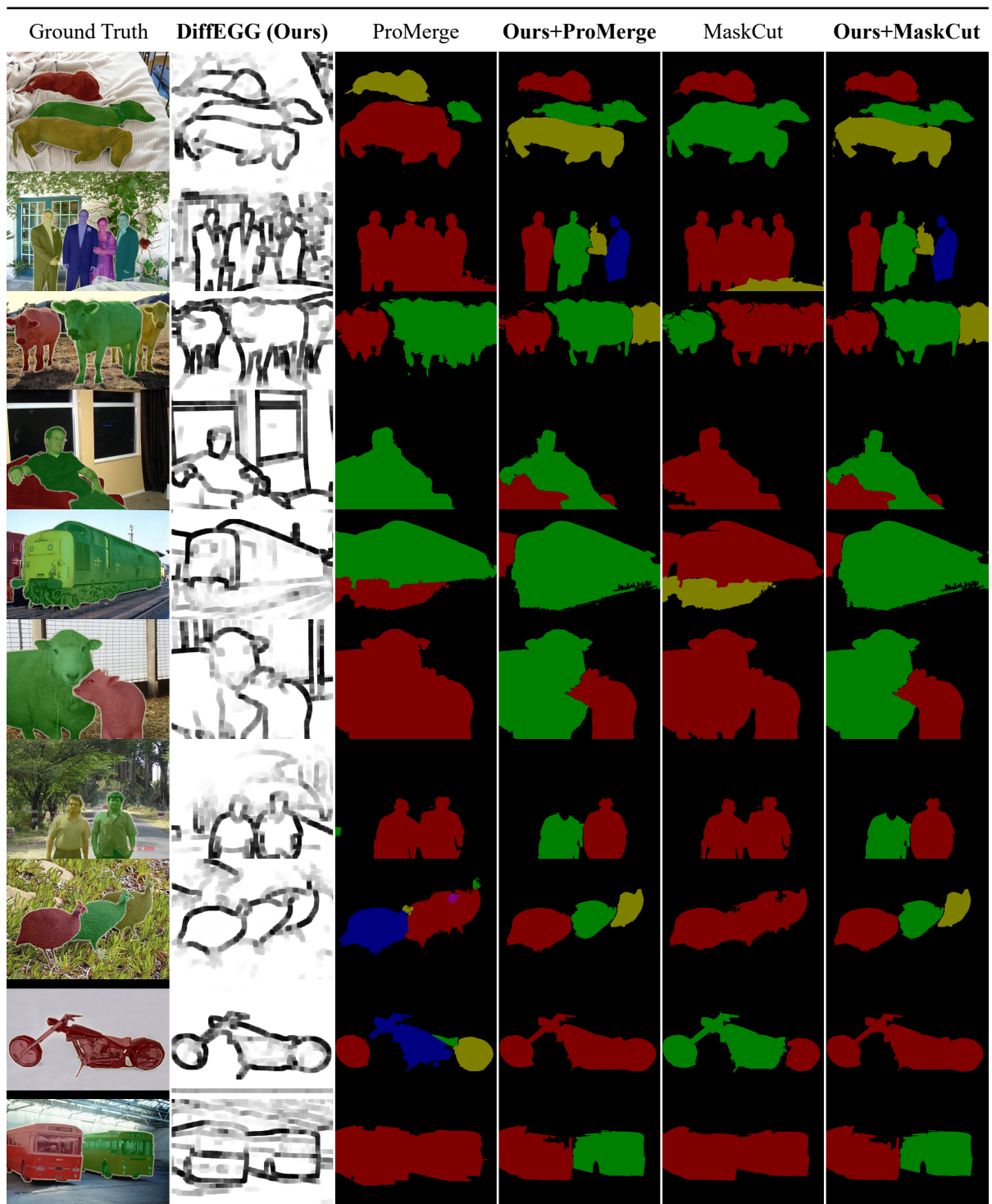


Figure P: Qualitative results in UIS with ours (DiffEGG+ProMerge, DiffEGG+MaskCut) and existing methods (ProMerge [36], MaskCut [67]) on the VOC2012 [15] validation set.

EdgeKL with Various Pretrained Models

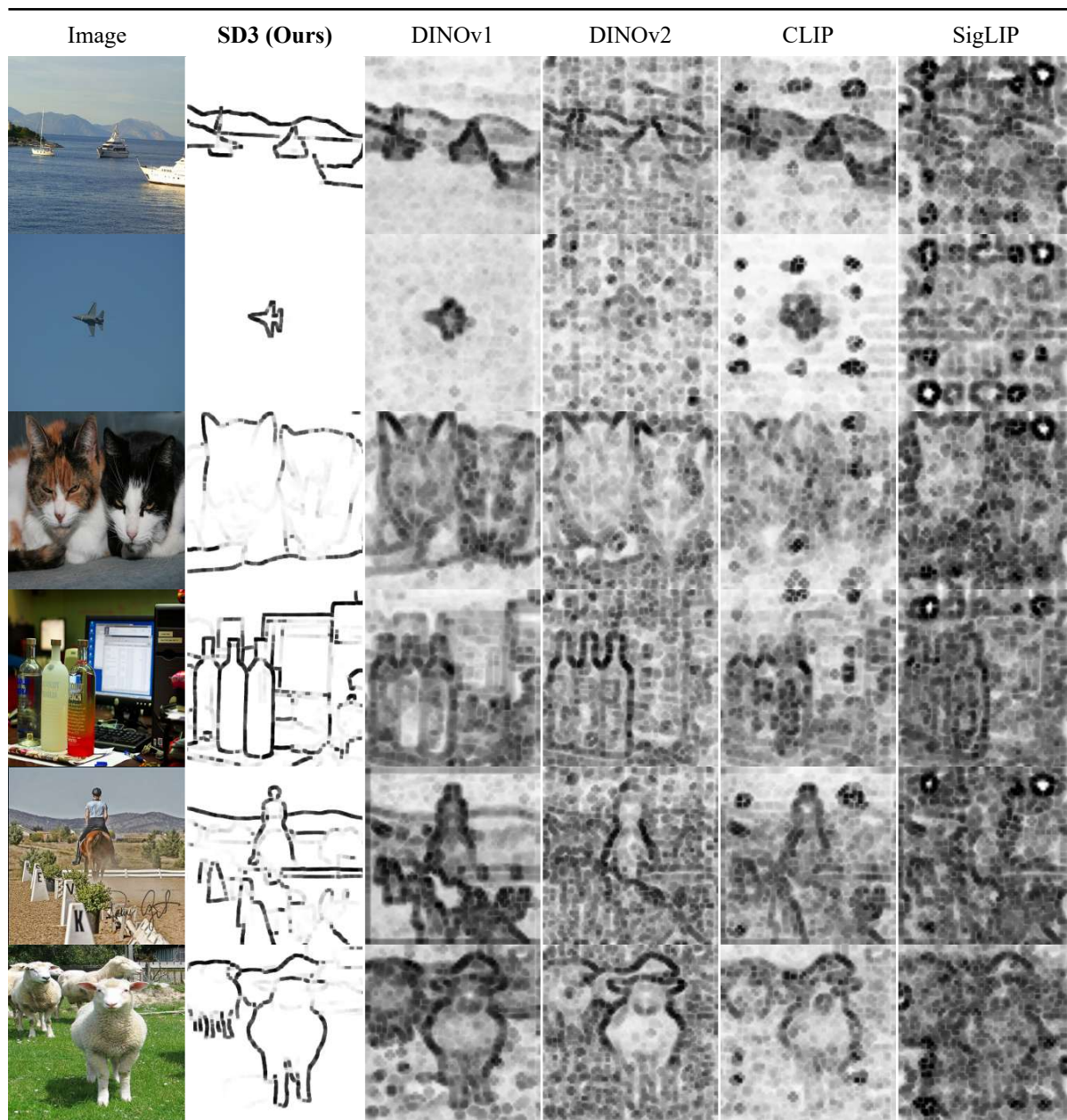


Figure Q: **EdgeKL with other backbones.** Feature maps from non-diffusion backbones are noisier and lower in resolution, which leads to suboptimal performance, as shown in Table 3. Despite these limitations, EdgeKL can detect initial edge maps from other backbones, from which noise and resolution issues can possibly be mitigated with fine-tuning and post-generation processing techniques.

F Acknowledgments

Kyungsu Kim is affiliated with the School of Transdisciplinary Innovations, Department of Biomedical Science, Medical Research Center, Interdisciplinary Program in Bioengineering, and Interdisciplinary Program in Artificial Intelligence at Seoul National University, Seoul, Republic of Korea.

This work was supported by a grant from the Institute of Information & Communications Technology Planning & Evaluation (IITP), funded by the Korean government (MSIT) [Grant No. RS2021-II211343, Artificial Intelligence Graduate School Program, Seoul National University]. Additionally, this research was conducted as part of the "AI Media and Cultural Enjoyment Expansion" Project, supported by the Ministry of Science and ICT and the National IT Industry Promotion Agency (NIPA) in 2025.

References

- [1] Jiwoon Ahn and Suha Kwak. Learning pixel-level semantic affinity with image-level supervision for weakly supervised semantic segmentation. In *The IEEE Conference on Computer Vision and Pattern Recognition (CVPR)*, 2018. 8, 6
- [2] Jiwoon Ahn, Sunghyun Cho, and Suha Kwak. Weakly supervised learning of instance segmentation with inter-pixel relations. In *The IEEE Conference on Computer Vision and Pattern Recognition (CVPR)*, 2019. 8, 6
- [3] Fan Bao, Shen Nie, Kaiwen Xue, Yue Cao, Chongxuan Li, Hang Su, and Jun Zhu. All are worth words: A vit backbone for diffusion models. In *Proceedings of the IEEE/CVF conference on computer vision and pattern recognition*, pages 22669–22679, 2023. 4, 5
- [4] Holger Caesar, Jasper Uijlings, and Vittorio Ferrari. COCO-Stuff: Thing and stuff classes in context. In *IEEE CVPR*, pages 1209–1218, 2018. 7, 8, 14
- [5] Mathilde Caron, Hugo Touvron, Ishan Misra, Hervé Jégou, Julien Mairal, Piotr Bojanowski, and Armand Joulin. Emerging properties in self-supervised vision transformers. In *IEEE ICCV*, pages 9650–9660, 2021. 4, 10, 1, 3
- [6] Junbum Cha, Jonghwan Mun, and Byungseok Roh. Learning to generate text-grounded mask for open-world semantic segmentation from only image-text pairs. In *IEEE CVPR*, pages 11165–11174, 2023. 5
- [7] Zhaozheng Chen, Tan Wang, Xiongwei Wu, Xian-Sheng Hua, Hanwang Zhang, and Qianru Sun. Class re-activation maps for weakly-supervised semantic segmentation. In *IEEE CVPR*, pages 969–978, 2022. 4, 3
- [8] Bowen Cheng, Alex Schwing, and Alexander Kirillov. Per-pixel classification is not all you need for semantic segmentation. *Advances in neural information processing systems*, 34:17864–17875, 2021. 4, 2
- [9] Bowen Cheng, Ishan Misra, Alexander G Schwing, Alexander Kirillov, and Rohit Girdhar. Masked-attention mask transformer for universal image segmentation. In *IEEE CVPR*, pages 1290–1299, 2022. 1, 4, 5, 9, 2
- [10] Arthur Daniel Costea, Andra Petrovai, and Sergiu Nedevschi. Fusion scheme for semantic and instance-level segmentation. In *2018 21st International Conference on Intelligent Transportation Systems (ITSC)*, pages 3469–3475, 2018. 1
- [11] Paul Couairon, Mustafa Shukor, Jean-Emmanuel Haugeard, Matthieu Cord, and Nicolas Thome. Diffcut: Catalyzing zero-shot semantic segmentation with diffusion features and recursive normalized cut, 2024. 5, 4
- [12] Songhe Deng, Wei Zhuo, Jinheng Xie, and Linlin Shen. Qa-clims: Question-answer cross language image matching for weakly supervised semantic segmentation. In *ACM MM*, pages 5572–5583, 2023. 4, 3
- [13] Omar Elharrouss, Somaya Al-Maadeed, Nandhini Subramanian, Najmath Ottakath, Noor Almaadeed, and Yassine Himeur. Panoptic segmentation: A review. *arXiv preprint arXiv:2111.10250*, 2021. 1
- [14] Patrick Esser, Sumith Kulal, Andreas Blattmann, Rahim Entezari, Jonas Müller, Harry Saini, Yam Levi, Dominik Lorenz, Axel Sauer, Frederic Boesel, Dustin Podell, Tim Dockhorn, Zion English, and Robin Rombach. Scaling rectified flow transformers for high-resolution image synthesis. In *Forty-first International Conference on Machine Learning*, 2024. 2, 3, 4, 5, 8, 10, 9
- [15] M. Everingham, S. M. A. Eslami, L. Van Gool, C. K. I. Williams, J. Winn, and A. Zisserman. The pascal visual object classes challenge: A retrospective. *International Journal of Computer Vision*, 111(1):98–136, 2015. 8, 1, 7, 10, 15

- [16] Junsong Fan, Zhaoxiang Zhang, and Tieniu Tan. Pointly-supervised panoptic segmentation. In *European Conference on Computer Vision*, pages 319–336. Springer, 2022. 3, 4, 9, 2
- [17] Ruochen Fan, Qibin Hou, Ming-Ming Cheng, Gang Yu, Ralph R Martin, and Shi-Min Hu. Associating inter-image salient instances for weakly supervised semantic segmentation. In *Proceedings of the European conference on computer vision (ECCV)*, pages 367–383, 2018. 3
- [18] Yuxin Fang, Quan Sun, Xinggang Wang, Tiejun Huang, Xinlong Wang, and Yue Cao. Eva-02: A visual representation for neon genesis. *Image and Vision Computing*, 149:105171, 2024. 10
- [19] Andreas Geiger, Philip Lenz, and Raquel Urtasun. Are we ready for autonomous driving? the kitti vision benchmark suite. In *2012 IEEE Conference on Computer Vision and Pattern Recognition*, pages 3354–3361, 2012. 7
- [20] Agrim Gupta, Piotr Dollar, and Ross Girshick. Lvis: A dataset for large vocabulary instance segmentation. In *Proceedings of the IEEE/CVF Conference on Computer Vision and Pattern Recognition (CVPR)*, 2019. 7
- [21] Mark Hamilton, Zhoutong Zhang, Bharath Hariharan, Noah Snavely, and William T. Freeman. Unsupervised semantic segmentation by distilling feature correspondences. In *ICLR*, 2022. 3
- [22] Kaiming He, Georgia Gkioxari, Piotr Dollár, and Ross B. Girshick. Mask r-cnn. In *2017 IEEE International Conference on Computer Vision (ICCV)*, pages 2980–2988, 2017. 8
- [23] Edward J Hu, Yelong Shen, Phillip Wallis, Zeyuan Allen-Zhu, Yuanzhi Li, Shean Wang, Lu Wang, and Weizhu Chen. LoRA: Low-rank adaptation of large language models. In *International Conference on Learning Representations*, 2022. 7
- [24] Taoseef Ishtiaq, Qing En, and Yuhong Guo. Exemplar-freesolo: Enhancing unsupervised instance segmentation with exemplars. In *Proceedings of the IEEE/CVF Conference on Computer Vision and Pattern Recognition*, pages 15424–15433, 2023. 4, 3
- [25] Guangfeng Jiang, Jun Liu, Yuzhi Wu, Wenlong Liao, Tao He, and Pai Peng. Mwsis: Multimodal weakly supervised instance segmentation with 2d box annotations for autonomous driving. In *Proceedings of the AAAI Conference on Artificial Intelligence*, pages 2507–2515, 2024. 4, 2
- [26] Sanghyun Jo, In-Jae Yu, and Kyungsu Kim. Recurseed and edgepredictmix: Single-stage learning is sufficient for weakly-supervised semantic segmentation. *arXiv preprint arXiv:2204.06754*, 2022. 4, 3
- [27] Sanghyun Jo, In-Jae Yu, and Kyungsu Kim. Mars: Model-agnostic biased object removal without additional supervision for weakly-supervised semantic segmentation. In *IEEE ICCV*, pages 614–623, 2023. 3, 4, 8, 9
- [28] Sanghyun Jo, Fei Pan, In-Jae Yu, and Kyungsu Kim. Dhr: Dual features-driven hierarchical rebalancing in inter- and intra-class regions for weakly-supervised semantic segmentation. In *European Conference on Computer Vision (ECCV)*, 2024. 1, 2, 3, 5, 8, 9, 10
- [29] Sanghyun Jo, Fei Pan, In-Jae Yu, and Kyungsu Kim. Dhr: Dual features-driven hierarchical rebalancing in inter- and intra-class regions for weakly-supervised semantic segmentation. In *European Conference on Computer Vision (ECCV)*, 2024. 4, 3
- [30] Beomyoung Kim, Youngjoon Yoo, Chae Eun Rhee, and Junmo Kim. Beyond semantic to instance segmentation: Weakly-supervised instance segmentation via semantic knowledge transfer and self-refinement. In *Proceedings of the IEEE/CVF conference on computer vision and pattern recognition*, pages 4278–4287, 2022. 3
- [31] Sangtae Kim, Daeyoung Park, and Byonghyo Shim. Semantic-aware superpixel for weakly supervised semantic segmentation. In *AAAI*, pages 1142–1150, 2023. 4, 3
- [32] Alexander Kirillov, Ross Girshick, Kaiming He, and Piotr Dollár. Panoptic feature pyramid networks. In *Proceedings of the IEEE/CVF conference on computer vision and pattern recognition*, pages 6399–6408, 2019. 4, 2
- [33] Alexander Kirillov, Eric Mintun, Nikhila Ravi, Hanzi Mao, Chloe Rolland, Laura Gustafson, Tete Xiao, Spencer Whitehead, Alexander C Berg, Wan-Yen Lo, et al. Segment anything. *arXiv preprint arXiv:2304.02643*, 2023. 5, 9, 7
- [34] Alex Krizhevsky, Ilya Sutskever, and Geoffrey E Hinton. Imagenet classification with deep convolutional neural networks. *NeurIPS*, 25:1097–1105, 2012. 5, 8, 7

- [35] Hyeokjun Kweon, Sung-Hoon Yoon, and Kuk-Jin Yoon. Weakly supervised semantic segmentation via adversarial learning of classifier and reconstructor. In *IEEE CVPR*, pages 11329–11339, 2023. 4, 3
- [36] Dylan Li and Gyungin Shin. Promerge: Prompt and merge for unsupervised instance segmentation. In *European Conference on Computer Vision (ECCV)*, 2024. 2, 4, 8, 9, 1, 3, 7, 11, 12, 13, 14, 15
- [37] Jing Li, Junsong Fan, and Zhaoxiang Zhang. Towards noiseless object contours for weakly supervised semantic segmentation. In *IEEE CVPR*, pages 16856–16865, 2022. 4, 3
- [38] Qizhu Li, Anurag Arnab, and Philip H.S. Torr. Weakly- and semi-supervised panoptic segmentation. In *Proceedings of the European Conference on Computer Vision (ECCV)*, 2018. 4, 2
- [39] Ruihuang Li, Chenhang He, Yabin Zhang, Shuai Li, Liyi Chen, and Lei Zhang. Sim: Semantic-aware instance mask generation for box-supervised instance segmentation. In *Proceedings of the IEEE/CVF Conference on Computer Vision and Pattern Recognition*, pages 7193–7203, 2023. 4, 2
- [40] Wentong Li, Yuqian Yuan, Song Wang, Jianke Zhu, Jianshu Li, Jian Liu, and Lei Zhang. Point2mask: Point-supervised panoptic segmentation via optimal transport. In *Proceedings of the IEEE/CVF International Conference on Computer Vision*, pages 572–581, 2023. 1, 2, 3, 4, 8, 9, 10
- [41] Yanwei Li, Hengshuang Zhao, Xiaojuan Qi, Liwei Wang, Zeming Li, Jian Sun, and Jiaya Jia. Fully convolutional networks for panoptic segmentation. In *Proceedings of the IEEE/CVF conference on computer vision and pattern recognition*, pages 214–223, 2021. 4, 9, 2
- [42] Zhiqi Li, Wenhai Wang, Enze Xie, Zhiding Yu, Anima Anandkumar, Jose M Alvarez, Ping Luo, and Tong Lu. Panoptic segformer: Delving deeper into panoptic segmentation with transformers. In *Proceedings of the IEEE/CVF conference on computer vision and pattern recognition*, pages 1280–1289, 2022. 4, 2
- [43] Justin Liang, Namdar Homayounfar, Wei-Chiu Ma, Yuwen Xiong, Rui Hu, and Raquel Urtasun. Polytransform: Deep polygon transformer for instance segmentation. In *2020 IEEE/CVF Conference on Computer Vision and Pattern Recognition (CVPR)*, pages 9128–9137, 2020. 9
- [44] Tsung-Yi Lin, Michael Maire, Serge Belongie, James Hays, Pietro Perona, Deva Ramanan, Piotr Dollár, and C. Lawrence Zitnick. Microsoft coco: Common objects in context. In *Computer Vision – ECCV 2014*, pages 740–755, Cham, 2014. Springer International Publishing. 8, 1, 7
- [45] Tsung-Yi Lin, Michael Maire, Serge Belongie, James Hays, Pietro Perona, Deva Ramanan, Piotr Dollár, and C Lawrence Zitnick. Microsoft COCO: Common objects in context. In *ECCV*, pages 740–755. Springer, 2014. 2, 11, 12, 13
- [46] Yuqi Lin, Minghao Chen, Wenxiao Wang, Boxi Wu, Ke Li, Binbin Lin, Haifeng Liu, and Xiaofei He. Clip is also an efficient segmenter: A text-driven approach for weakly supervised semantic segmentation. In *IEEE CVPR*, pages 15305–15314, 2023. 4, 3
- [47] Haotian Liu, Chunyuan Li, Qingyang Wu, and Yong Jae Lee. Visual instruction tuning. *Advances in neural information processing systems*, 36, 2024. 9, 10
- [48] Sheng Liu, Kangning Liu, Weicheng Zhu, Yiqiu Shen, and Carlos Fernandez-Granda. Adaptive early-learning correction for segmentation from noisy annotations. In *IEEE CVPR*, pages 2606–2616, 2022. 4, 3
- [49] Shilong Liu, Zhaoyang Zeng, Tianhe Ren, Feng Li, Hao Zhang, Jie Yang, Chunyuan Li, Jianwei Yang, Hang Su, Jun Zhu, et al. Grounding dino: Marrying dino with grounded pre-training for open-set object detection. *arXiv preprint arXiv:2303.05499*, 2023. 5, 9
- [50] Quang Nguyen, Truong Vu, Anh Tran, and Khoi Nguyen. Dataset diffusion: Diffusion-based synthetic data generation for pixel-level semantic segmentation. In *Advances in Neural Information Processing Systems*, pages 76872–76892. Curran Associates, Inc., 2023. 4
- [51] Dantong Niu, Xudong Wang, Xinyang Han, Long Lian, Roei Herzig, and Trevor Darrell. Unsupervised universal image segmentation. In *Proceedings of the IEEE/CVF Conference on Computer Vision and Pattern Recognition*, pages 22744–22754, 2024. 4, 1, 3
- [52] Maxime Oquab, Timothée Darcet, Theo Moutakanni, Huy V. Vo, Marc Szafraniec, Vasil Khalidov, Pierre Fernandez, Daniel Haziza, Francisco Massa, Alaaeldin El-Nouby, Russell Howes, Po-Yao Huang, Hu Xu, Vasu Sharma, Shang-Wen Li, Wojciech Galuba, Mike Rabbat, Mido Assran, Nicolas Ballas, Gabriel Synnaeve, Ishan Misra, Herve Jegou, Julien Mairal, Patrick Labatut, Armand Joulin, and Piotr Bojanowski. Dinov2: Learning robust visual features without supervision, 2023. 10

- [53] William Peebles and Saining Xie. Scalable diffusion models with transformers. In *Proceedings of the IEEE/CVF International Conference on Computer Vision*, pages 4195–4205, 2023. 4, 5
- [54] Sida Peng, Wen Jiang, Huaijin Pi, Xiuli Li, Hujun Bao, and Xiaowei Zhou. Deep snake for real-time instance segmentation. In *CVPR*, 2020. 9
- [55] Dustin Podell, Zion English, Kyle Lacey, Andreas Blattmann, Tim Dockhorn, Jonas Müller, Joe Penna, and Robin Rombach. Sdxl: Improving latent diffusion models for high-resolution image synthesis, 2023. 2, 4, 5, 10, 9
- [56] Alec Radford, Jong Wook Kim, Chris Hallacy, Aditya Ramesh, Gabriel Goh, Sandhini Agarwal, Girish Sastry, Amanda Askell, Pamela Mishkin, Jack Clark, et al. Learning transferable visual models from natural language supervision. In *ICML*, pages 8748–8763. PMLR, 2021. 4, 5
- [57] Robin Rombach, Andreas Blattmann, Dominik Lorenz, Patrick Esser, and Björn Ommer. High-resolution image synthesis with latent diffusion models. In *Proceedings of the IEEE/CVF conference on computer vision and pattern recognition*, pages 10684–10695, 2022. 9, 10
- [58] Shenghai Rong, Bohai Tu, Zilei Wang, and Junjie Li. Boundary-enhanced co-training for weakly supervised semantic segmentation. In *IEEE CVPR*, pages 19574–19584, 2023. 4, 3
- [59] Azriel Rosenfeld and John L Pfaltz. Sequential operations in digital picture processing. *Journal of the ACM (JACM)*, 13(4):471–494, 1966. 8
- [60] Lixiang Ru, Heliang Zheng, Yibing Zhan, and Bo Du. Token contrast for weakly-supervised semantic segmentation. In *IEEE CVPR*, pages 3093–3102, 2023. 4, 3
- [61] Shuai Shao, Zeming Li, Tianyuan Zhang, Chao Peng, Gang Yu, Xiangyu Zhang, Jing Li, and Jian Sun. Objects365: A large-scale, high-quality dataset for object detection. In *Proceedings of the IEEE/CVF International Conference on Computer Vision (ICCV)*, 2019. 7
- [62] Yunhang Shen, Liujuan Cao, Zhiwei Chen, Feihong Lian, Baochang Zhang, Chi Su, Yongjian Wu, Feiyue Huang, and Rongrong Ji. Toward joint thing-and-stuff mining for weakly supervised panoptic segmentation. In *Proceedings of the IEEE/CVF Conference on Computer Vision and Pattern Recognition*, pages 16694–16705, 2021. 1, 9, 3
- [63] Yang Song, Jascha Sohl-Dickstein, Diederik P Kingma, Abhishek Kumar, Stefano Ermon, and Ben Poole. Score-based generative modeling through stochastic differential equations. In *International Conference on Learning Representations*, 2021. 5
- [64] Junjiao Tian, Lavisha Aggarwal, Andrea Colaco, Zsolt Kira, and Mar Gonzalez-Franco. Diffuse attend and segment: Unsupervised zero-shot segmentation using stable diffusion. In *Proceedings of the IEEE/CVF Conference on Computer Vision and Pattern Recognition (CVPR)*, pages 3554–3563, 2024. 5, 4
- [65] Xinlong Wang, Rufeng Zhang, Chunhua Shen, Tao Kong, and Lei Li. Dense contrastive learning for self-supervised visual pre-training. In *Proc. IEEE Conf. Computer Vision and Pattern Recognition (CVPR)*, 2021. 4, 3
- [66] Xinlong Wang, Zhiding Yu, Shalini De Mello, Jan Kautz, Anima Anandkumar, Chunhua Shen, and Jose M Alvarez. Freesolo: Learning to segment objects without annotations. In *Proceedings of the IEEE/CVF conference on computer vision and pattern recognition*, pages 14176–14186, 2022. 4, 3
- [67] Xudong Wang, Rohit Girdhar, Stella X Yu, and Ishan Misra. Cut and learn for unsupervised object detection and instance segmentation. In *Proceedings of the IEEE/CVF conference on computer vision and pattern recognition*, pages 3124–3134, 2023. 2, 3, 4, 8, 9, 10, 1, 5, 7, 11, 12, 13, 14, 15
- [68] Xudong Wang, Ishan Misra, Ziyun Zeng, Rohit Girdhar, and Trevor Darrell. Videocutler: Surprisingly simple unsupervised video instance segmentation. In *Proceedings of the IEEE/CVF Conference on Computer Vision and Pattern Recognition*, pages 22755–22764, 2024. 4, 1, 3
- [69] Yangtao Wang, Xi Shen, Yuan Yuan, Yuming Du, Maomao Li, Shell Xu Hu, James L Crowley, and Dominique Vaufreydaz. Tokencut: Segmenting objects in images and videos with self-supervised transformer and normalized cut. *IEEE transactions on pattern analysis and machine intelligence*, 2023. 4, 1, 7
- [70] Weijia Wu, Yuzhong Zhao, Hao Chen, Yuchao Gu, Rui Zhao, Yefei He, Hong Zhou, Mike Zheng Shou, and Chunhua Shen. Datasetdm: Synthesizing data with perception annotations using diffusion models. In *Advances in Neural Information Processing Systems*, pages 54683–54695. Curran Associates, Inc., 2023. 4

- [71] Tete Xiao, Yingcheng Liu, Bolei Zhou, Yuning Jiang, and Jian Sun. Unified perceptual parsing for scene understanding. In *European Conference on Computer Vision*. Springer, 2018. 7, 5
- [72] Jinheng Xie, Jianfeng Xiang, Junliang Chen, Xianxu Hou, Xiaodong Zhao, and Linlin Shen. C2am: Contrastive learning of class-agnostic activation map for weakly supervised object localization and semantic segmentation. In *IEEE CVPR*, pages 989–998, 2022. 4, 3
- [73] Jiarui Xu, Sifei Liu, Arash Vahdat, Wonmin Byeon, Xiaolong Wang, and Shalini De Mello. Open-vocabulary panoptic segmentation with text-to-image diffusion models. In *Proceedings of the IEEE/CVF Conference on Computer Vision and Pattern Recognition (CVPR)*, pages 2955–2966, 2023. 4, 2
- [74] Lian Xu, Wanli Ouyang, Mohammed Bennamoun, Farid Boussaid, and Dan Xu. Multi-class token transformer for weakly supervised semantic segmentation. In *IEEE CVPR*, pages 4310–4319, 2022. 4, 3
- [75] Muiyang Yi, Quan Cui, Hao Wu, Cheng Yang, Osamu Yoshie, and Hongtao Lu. A simple framework for text-supervised semantic segmentation. In *Proceedings of the IEEE/CVF Conference on Computer Vision and Pattern Recognition (CVPR)*, pages 7071–7080, 2023. 4, 3
- [76] Haoxuan You, Haotian Zhang, Zhe Gan, Xianzhi Du, Bowen Zhang, Zirui Wang, Liangliang Cao, Shih-Fu Chang, and Yinfei Yang. Ferret: Refer and ground anything anywhere at any granularity. *arXiv preprint arXiv:2310.07704*, 2023. 5, 9
- [77] Oliver Zendel, Matthias Schörrhuber, Bernhard Rainer, Markus Murschitz, and Csaba Beleznai. Unifying panoptic segmentation for autonomous driving. In *Proceedings of the IEEE/CVF Conference on Computer Vision and Pattern Recognition*, pages 21351–21360, 2022. 1
- [78] Wenwei Zhang, Jiangmiao Pang, Kai Chen, and Chen Change Loy. K-net: Towards unified image segmentation. *Advances in Neural Information Processing Systems*, 34:10326–10338, 2021. 4, 2
- [79] Bolei Zhou, Aditya Khosla, Agata Lapedriza, Aude Oliva, and Antonio Torralba. Learning deep features for discriminative localization. In *IEEE CVPR*, pages 2921–2929, 2016. 3
- [80] Chong Zhou, Chen Change Loy, and Bo Dai. Extract free dense labels from clip. In *ECCV*, pages 696–712. Springer, 2022. 5
- [81] Yanzhao Zhou, Yi Zhu, Qixiang Ye, Qiang Qiu, and Jianbin Jiao. Weakly supervised instance segmentation using class peak response. In *Proceedings of the IEEE conference on computer vision and pattern recognition*, pages 3791–3800, 2018. 3
- [82] Lianghui Zhu, Yingyue Li, Jieming Fang, Yan Liu, Hao Xin, Wenyu Liu, and Xinggang Wang. Weaktr: Exploring plain vision transformer for weakly-supervised semantic segmentation. *arXiv preprint arXiv:2304.01184*, 2023. 4, 3